Journal of Applied Physics

RESEARCH ARTICLE | JULY 23 2021

Wurtzite ScAlN, InAlN, and GaAlN crystals, a comparison of structural, elastic, dielectric, and piezoelectric properties

Special Collection: Wide Bandgap Semiconductor Materials and Devices

O. Ambacher ✉ ; B. Christian; N. Feil ; D. F. Urban ; C. Elsässer ; M. Prescher; L. Kirste

J. Appl. Phys. 130, 045102 (2021)
https://doi.org/10.1063/5.0048647

Journal of Applied Physics ARTICLE scitation.org/journal/jap

Wurtzite ScAlN, InAlN, and GaAlN crystals, a comparison of structural, elastic, dielectric, and piezoelectric properties

Cite as: J. Appl. Phys. **130**, 045102 (2021); doi: 10.1063/5.0048647
Submitted: 25 February 2021 · Accepted: 7 July 2021 ·
Published Online: 23 July 2021

O. Ambacher,[1,2,a] B. Christian,[1] N. Feil,[1] D. F. Urban,[3] C. Elsässer,[3] M. Prescher,[2] and L. Kirste[2]

AFFILIATIONS

[1]Institute for Sustainable Systems Engineering (INATECH), Albert-Ludwigs-University Freiburg, Emmy-Noether-Str. 2, D-79110 Freiburg, Germany
[2]Fraunhofer Institute for Applied Solid State Physics, Tullastr. 72, D-79108 Freiburg, Germany
[3]Fraunhofer Institute for Mechanics of Materials, Wöhlerstr. 11, D-79108 Freiburg, Germany

Note: This paper is part of the Special Topic on Wide Bandgap Semiconductor Materials and Devices.
[a]**Author to whom correspondence should be addressed:** oliver.ambacher@iaf.fraunhofer.de

ABSTRACT

We present detailed investigations of the structural, elastic, dielectric, and piezoelectric properties of scandium aluminum nitride ($Sc_xAl_{1-x}N$) with the wurtzite crystal structure by means of first-principles calculations based on density functional theory in order to enable a detailed comparison to the corresponding physical properties of GaAlN and InAlN. The goal of our approach is to use atomistic simulations to extract the novel solid state characteristics of $Sc_xAl_{1-x}N$ crystals by the determination of complete sets of coefficients for the elastic, compliance, and piezoelectric tensor and to confirm the theoretical predictions by experimental measurements of selected tensor coefficients. The calculation of the tensor components is accompanied by a detailed analysis of the crystal structures, e.g., average bond length, bond angles, lattice parameters, and mass density in dependence on alloy composition of $Sc_xAl_{1-x}N$. If an increasing number of Al atoms of up to $x = 0.5$ are replaced by Sc atoms, we observe a nonlinear change of the ratio of lattice parameter $\frac{c(x)}{a(x)}$ and average bond angles of about 10% and 5%, respectively, which give an indication of an increasing deviation of the crystal structure of $Sc_xAl_{1-x}N$ from an ideal hexagonal lattice. As a consequence of the deformed crystal structure and the iconicity of the Sc–N bond, we predict a change in value of the elastic coefficient $C_{33}^{ScAlN}(x)$, the piezoelectric coefficient $e_{33}^{ScAlN}(x)$, and the value of spontaneous polarization $P_{SP}^{ScAlN}(x)$ of up to 65%, 150%, and 230%, respectively. Based, on these simulation results, physical features of practical use are derived, like the average bulk, shear, and the Young modulus as well as the reciprocal Young's modulus and Poisson ratio. Furthermore, the spontaneous polarization of $Sc_xAl_{1-x}N$ is approximated, taking nonlinear effects into account as well as the piezoelectric polarization caused by uniaxial, biaxial, and hydrostatic stresses in dependency on alloy composition and strain. A detailed comparison of the structural and polarization related properties of GaAlN and InAlN allows us to point out the peculiarity of wurtzite ScAlN crystals within the group III-nitrides.

I. INTRODUCTION

Microelectronic energy harvester and acoustic wave devices operate on the basis of the piezoelectric effect, in which mechanical energy is transferred to electrical energy or vice versa.[1,2] The performance of a piezoelectric microelectromechanical system or a piezo-acoustic wave device is determined by the properties of the active layer, such as the piezoelectric coefficients, electromechanical coupling, and mechanical quality factor.[3] The energy efficiency and power output of these devices is proportional to the piezoelectric polarization and mechanical stiffness but decreases with higher dielectric coefficient. Ferroelectric single crystals like $La_3Ga_5SiO_{14}$ and $PbZr_xTi_{1-x}O_3$ have very high piezoelectric response and electromechanical coupling coefficients, which makes them suitable for device applications.[4] However, high dielectric constants counterbalance these advantages in terms of efficiency and power output. Accordingly, materials with power outputs similar to that of $Pb[Zr_xTi_{1-x}]O_3$ but free of Pb, received more scientific and

technological interest, recently. Aluminum nitride (AlN) based thin films offer promising alternatives due to comparable power output combined with an extremely high quality factor. Furthermore, its piezoelectric response has a high temperature stability up to 1150 °C.[5] The major drawback of wurtzite AlN is that it exhibits a low piezoelectric modulus of $d_{33} = 5.5$ pC/N in comparison to 410 pC/N of $PbZr_xTi_{1-x}O_3$. $Sc_xAl_{1-x}N$ alloys were found experimentally to have a giant increase of the piezoelectric moduli d_{33} up to $x = 0.45$ in reference to pure wurtzite AlN.[6] Up to date, most ScAlN resonator studies[7] have focused on the low Sc concentration region ($x \leq 0.15$), probably either because the acoustic wave attenuation loss ($1/Q$ factor) related to the decrease in stiffness for high Sc concentration was expected to be too large for use as practical resonators or because it is difficult to realize high structural quality films at high alloy compositions. However, GHz surface acoustic wave filters with high a Q value of 660 are reported for a high Sc concentration film on a SiC substrate structure.[8] Furthermore, Yanagatani and Suzuki[9] have obtained a significant increase of the coupling coefficient from $k_t^2 = 6.4\%$–14% by enhancement of Sc concentration up to $x = 0.38$, proving the potential of thin ScAlN films for high frequency acoustic wave devices. These outstanding results motivate this article in which we present elastic, dielectric, and piezoelectric properties of ScAlN with the wurtzite crystal structure using first-principles calculations based on density functional theory (DFT) added by a detailed experimental analysis of structural, mechanical, and polarization related effects. The goal of our approach is to use atomistic simulations to extract the whole set of tensor components and to confirm the theoretical predictions by a complement experimental analysis of ScAlN thin films in order to enable a detailed comparison of ScAlN to the physical properties of randomly alloyed GaAlN and InAlN ternary compounds. The comparison presented include, e.g., the lattice parameters, internal cell parameter, piezoelectric and stiffness coefficients, Young's and bulk modulus, mass density, as well as piezoelectric and spontaneous polarization for alloy compositions of up to $x = 0.5$. We point out novel properties of ScAlN in comparison to the related ternary nitrides InAlN and GaAlN in order to stimulate new designs of application related micromechanical, piezo-acoustic, as well as electronic devices.

II. DENSITY FUNCTIONAL THEORY SIMULATION

The structure of ScAlN wurtzite crystals as well as their elastic and piezoelectric coefficients are simulated by density functional theory (DFT)[10] based on supercells representative for random alloys. These cells are characterized by Al and Sc atoms sharing the same sublattice without giving rise to long range order, containing a limited number of atoms in combination with periodic boundary conditions. The structure model of finite size is biased by the choice of the specific disorder representation. To overcome this problem, a large variety of different supercells for each chemical composition x were simulated, accompanied, and by an appropriate averaging procedure to extract the physical properties of relevance. Supercells which contain 36 atoms where chosen to simulate $Sc_xAl_{1-x}N$ random alloy with $0 \leq x \leq 0.5$. The calculation of elastic and piezoelectric constants was carried out using the PWscf code of the Quantum Espresso software package[11,12] using the generalized gradient approximation of Perdew–Burke–Ernzerhof (GGA-PBE) for exchange-correlation. The wave functions of the valence electrons are represented by a plane waves basis set with a cutoff energy of 55 Ry, and the electron density and effective Kohn–Sham potential by discrete Fourier series with a cutoff energy of 440 Ry. The interactions of valence electrons with the atomic nuclei and core electrons are described by pseudopotentials taken from the open-source standard solid state pseudopotentials library.[13,14] Here, ultrasoft pseudopotentials are chosen for N and Sc atoms, while the pseudopotential for Al is of projector augmented wave type. Brillouin-zone integrals for the 36 atoms supercells are evaluated on a Monkhorst–Pack mesh of $3 \times 3 \times 6$ k-points with a Gaussians smearing of 0.01 Ry. The convergence threshold was set to 10^{-5} Ry for the total energy and to 10^{-4} Ry/Bo (1 Bohr = 0.529 Å) for the forces on atoms. Elastic stresses and interatomic forces were relaxed using the Broyden–Fletcher–Goldfarb–Shanno algorithm. The choice of the representative set of disorder configurations is guided by comparing the DFT total energies of the various possible atomic configurations at fixed x. The total energies determined are the ground-state energies of the structurally optimized supercell models, which are obtained by relaxation of the atom positions and the cell shape to zero elastic stress and zero atomic forces. In other words, the lattice constants and atomic coordinates are determined such that the total energy is minimal for the given distribution of Al and Sc atoms on the metal sublattice.

III. GROWTH AND STRUCTURAL PROPERTIES

To enable a comparison of theoretical predictions[10,17] and experimental measurements regarding the structural properties of wurtzite ScAlN crystals with the data published for InAlN and GaAlN crystals,[15–20] we prepared nitrogen and metal polar $Sc_xAl_{1-x}N$ films with thicknesses between 500 and 1500 nm and Sc concentrations of up to $x = 0.4$ by reactive magnetron co-sputtering. The polarity of the films was controlled by the surface termination of the Si and Al_2O_3 substrates and determined by etching experiments and transmission electron microscopy. The targets have been 100 mm diameter plates of Sc and Al of 99.9% and 99.999% purity, respectively. The system applied was pumped down to a base pressure below 10^{-6} mbar before admitting highly purified nitrogen and argon gas at a flux ratio of $Ar/N_2 = 1/2$ into the reactor. The films were grown on rotating 6-in. Si(001) or 4-in. Al_2O_3(0001) substrates at chuck temperatures between 300 and 350 °C in 4×10^{-3} mbar gas pressure with an average substrate–target distance of about 50 mm. The cathode power was varied between 700 and 1000 W for the Al-target and between 200 and 860 W for the Sc-target, respectively, resulting in deposition rates between 0.15 and 0.23 nm/s.[21] After deposition, the samples were investigated by secondary ion mass spectrometry (SIMS) and energy dispersive x-ray spectroscopy (EDX) to determine the Sc content of the films. High-resolution x-ray diffraction (HRXRD) and atomic force microscopy (AFM) were used to check for the structural quality. Only samples with a rocking curve full width of half maximum (FWHM) of the 0002 reflex below 2° and a surface roughness of less than rms < 10 nm (scanned area $2 \times 2\,\mu m^2$) have been considered for further investigations. Additionally, symmetric ($2\theta/\theta$) as well as asymmetric ($2\theta/\omega$) HRXRD scans were conducted in order to determine the lattice parameters $a(x)$ and $c(x)$ using a

method, described in Ref. 22. In the asymmetric configuration, the $10\bar{1}5$ reflections were recorded at shallow and steep incidence angle ω for the determination of lattice parameter $a(x)$, while the $c(x)$-lattice parameter was determined from the angle of the 0002 reflection in a symmetric scan. The measured and simulated lattice parameters $a(x)$, $c(x)$ and the $c(x)/a(x)$ ratio as well as comparable data available in the literature are shown in Figs. 1–3, respectively.[15–18,23,24] The lattice parameters $a(x)$ and $c(x)$ of $Ga_xAl_{1-x}N$ and $In_xAl_{1-x}N$ obtained in Ref. 19 follow Vegard's law,[25] meaning, the lattice parameters (given in Å) are increasing linearly in dependence on the concentration of Ga or In atoms substituting Al atoms in the crystal lattice,[19]

$$a^{\mathrm{GaAlN}}(x) = (3.1095 + 0.0891\,x), \tag{1a}$$

$$a^{\mathrm{InAlN}}(x) = (3.1095 + 0.4753\,x), \tag{1b}$$

$$c^{\mathrm{GaAlN}}(x) = (4.9939 + 0.2323\,x), \tag{1c}$$

$$c^{\mathrm{InAlN}}(x) = (4.9939 + 0.8063\,x). \tag{1d}$$

It should be mentioned that Darakchieva *et al.* observed an increase of $a^{\mathrm{InAlN}}(x)$ and $c^{\mathrm{InAlN}}(x)$ with increasing In content showing a very small nonlinear effect which is neglected in the following discussion.[20] In opposite to $Ga_xAl_{1-x}N$ and $In_xAl_{1-x}N$ but in agreement with Zhang *et al.*,[17] our theory predicts a pronounced nonlinear behavior of the lattice parameters in the case of $Sc_xAl_{1-x}N$. For the description of the simulated and experimentally observed nonlinearities of structural (and later on other physical) properties, we have

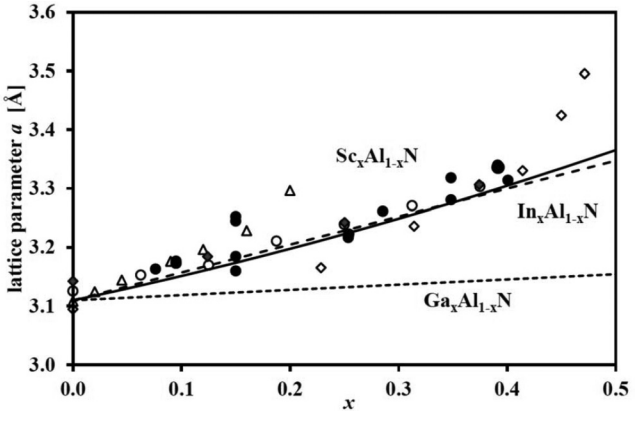

FIG. 1. Measured and simulated lattice parameter $a(x)$ (symbols: black circles: own experimental results, black rhombus,[15] open circles,[17] open square,[18] open triangle,[23] and open rhombus[24]) as well as approximated lattice parameter $a(x)$ [continuous line, Eq. (3a)] vs alloy composition of $Sc_xAl_{1-x}N$. The linear interpolation of lattice parameter between the two relevant binary nitrides (Vegard's law) for $Ga_xAl_{1-x}N$ and $In_xAl_{1-x}N$ (dashed lines[19]) are shown for comparison.

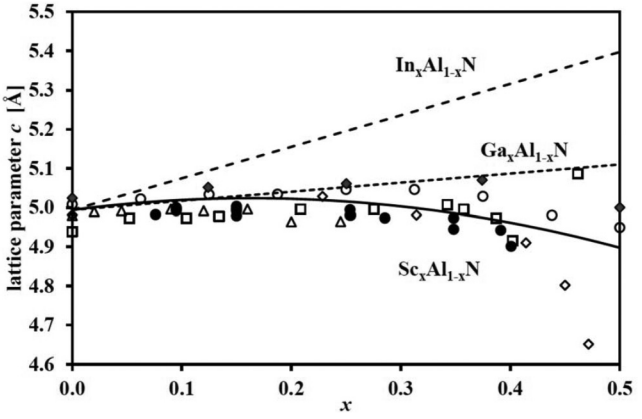

FIG. 2. Measured and simulated lattice parameter $c(x)$ (symbols as in Fig. 1) as well as approximated lattice parameter $c(x)$ [continuous line, Eq. (3b)] vs alloy composition of $Sc_xAl_{1-x}N$. The linear interpolation of lattice parameter between the two relevant binary nitrides (Vegard's law) for $Ga_xAl_{1-x}N$ and $In_xAl_{1-x}N$ (dashed lines[19]) are shown for comparison.

chosen an approximation by quadratic equations of the form,

$$Y^{\mathrm{MeAlN}}(x) = Y^{\mathrm{MeN}}x + Y^{\mathrm{AlN}}(1-x) + bx(1-x), \tag{2a}$$

where

$$b = 4Y^{\mathrm{MeAlN}}(x = 0.5) - 2(Y^{\mathrm{MeN}} + Y^{\mathrm{AlN}}) \tag{2b}$$

is the bowing parameter and Me = Sc, and Ga, In. In the case of wurtzite $Sc_xAl_{1-x}N$, our theoretical approximation as well as the experimental measurements are restricted to Sc concentrations $0 \le x \le 0.5$

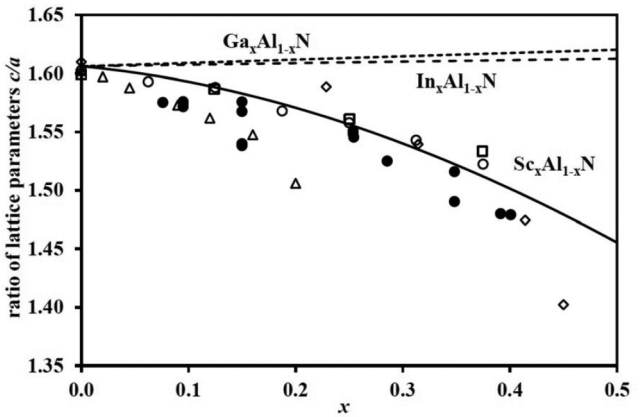

FIG. 3. Measured and simulated (symbols as in Fig. 1) as well as approximated ratio of lattice parameters $c(x)/a(x)$ (continuous line) vs alloy composition of $Sc_xAl_{1-x}N$. The values for $Ga_xAl_{1-x}N$ and $In_xAl_{1-x}N$ (dashed lines) are shown for comparison.

mainly because of the phase transition to the cubic structure observed at about $x = 0.45 \pm 0.05$.[26] The quadratic equations (3a) and (3b) describing lattice parameter $a^{\mathrm{ScAlN}}(x)$ and $c^{\mathrm{ScAlN}}(x)$ are approximations to the data simulated by Urban *et al.*[10] as described in Chap. I, rescaled to the lattice constants of AlN (given in Å),[19]

$$a^{\mathrm{ScAlN}}(x) = (3.741\,x + 3.110(1-x) - 0.242\,x\,(1-x)), \tag{3a}$$

$$c^{\mathrm{ScAlN}}(x) = (4.245\,x + 4.994\,(1-x) + 1.114\,x\,(1-x)). \tag{3b}$$

The value of the bowing parameter for $a^{\mathrm{ScAlN}}(x)$ is much smaller in comparison to that of $c^{\mathrm{ScAlN}}(x)$, and as consequence, the ratio of lattice parameters $c(x)/a(x)$ also show a nonlinear dependence on Sc content (Figs. 1–3). Experimental data for ScAlN and the $c(x)/a(x)$-ratios of GaAlN and InAlN are shown for comparison in Fig. 3. While for GaAlN and InAlN, the ratio of lattice parameters increases in a linear manner toward the c/a value of an ideal wurtzite crystal, if an enlarged number of Al atoms are substituted by Ga or In, it deviates significantly and in a strongly nonlinear manner, if Al atoms are substituted by Sc. The predicted $c(x)/a(x)$-values are slightly above the ones determined by high-resolution x-ray diffraction and also higher in comparison to the experimental data present in the literature. In our case, the experimental values can differ from the predicted ones because of the biaxial strain in the ScAlN films caused by the thermal and lattice mismatch toward the substrates, which will be discussed in more detail in Chap. VI.

We have used high-resolution x-ray diffraction and x-ray reflectivity to determine the mass density of ScAlN in dependence of its Sc content.[22] The experimental results are shown in Fig. 4 and compared to the mass density calculated from the lattice parameters $a^{\mathrm{MeAlN}}(x)$ and $c^{\mathrm{MeAlN}}(x)$ ($\mathrm{Me}_x\mathrm{Al}_{1-x}\mathrm{N}$, Me = Sc, Ga, or In) as described by Refs. 27–29. The density of a hexagonal ternary crystal can be determined by the ratio,

$$\rho^{\mathrm{MeAlN}}(x) = \frac{m_{uc}^{\mathrm{MeAlN}}(x)}{V_{uc}^{\mathrm{MeAlN}}(x)}, \tag{4}$$

where

$$m_{\mathrm{uc}}^{\mathrm{MeAlN}}(x) = \frac{Z^{*}\mathrm{u}}{N_A}(m_{\mathrm{Me}}x + m_{\mathrm{Al}}(1-x) + m_N), \tag{5}$$

is the mass of the unit cell, with $Z = 2$, $\mathrm{u} = 1.660\,54 \times 10^{-24}\,\frac{\mathrm{g}}{\mathrm{mol}}$, $N_A = 6.022\ 10^{-23}\,\frac{1}{\mathrm{mol}}$, $m_{\mathrm{Al}} = 26.982$, $m_{\mathrm{N}} = 14.007$, $m_{\mathrm{Sc}} = 44.956$, $m_{\mathrm{Ga}} = 69.723$, $m_{\mathrm{In}} = 114.818$, and

$$V_{\mathrm{uc}}^{\mathrm{MeAlN}}(x) = \frac{\sqrt{3}}{2}a^{\mathrm{MeAlN}}(x)^2 c^{\mathrm{MeAlN}}(x) \tag{6}$$

the volume of the unit cell. From Fig. 4, it can be seen that the mass density of GaAlN and InAlN is increasing, if an increasing number of Al atoms are substituted by the heavier Ga and In atoms. The density of GaInN and InAlN is enlarged by 44.5% and 65.4%, if half of the Al atoms are replaced by Ga or In, respectively. The experimental as well as the calculated data indicate only a small increase of the mass density for ScAlN for x up to 0.5. The mass and the volume of the ScAlN unit cell are increased by 22% and 14%, respectively, resulting in an enlargement of the mass density of only 6% in the same range of composition. If the calculated mass densities of the ternary compounds are approximated by quadratic functions (in units of $\mathrm{g/cm^3}$), we obtain

$$\rho^{\mathrm{GaAlN}}(x) = 6.005\,x + 3.255\,(1-x) + 0.300\,x\,(1-x), \tag{7a}$$

$$\rho^{\mathrm{InAlN}}(x) = 6.628\,x + 3.255\,(1-x) + 1.744\,x\,(1-x), \tag{7b}$$

$$\rho^{\mathrm{ScAlN}}(x) = 3.806\,x + 3.255\,(1-x) - 0.298\,x\,(1-x). \tag{7c}$$

It can be recognized that beside the mass density also the bowing parameters of GaAlN and InAlN in comparison to ScAlN are significantly larger. The relative low mass density of AlN and its small increase with Sc incorporation combined with the expected enlargement of the piezoelectric effect by substitution of Al atoms by Sc atoms (discussed in Chap. VI) is of advantage for piezoelectric microelectromechanical systems and piezo-acoustic wave devices. This advantage can be partly reduced by a corresponding increase of the dielectric constant. For these reasons, we have measured the dielectric constant $\varepsilon_{33}(x)$ of $\mathrm{Sc}_x\mathrm{Al}_{1-x}\mathrm{N}$ by capacity–voltage profiling[26] and compared our data to the experimental results available in the literature[9,26,30] as well as to the data published for GaAlN and InAlN[19] (Fig. 5). The dielectric constant $\varepsilon_{33}(x)$ of GaAlN is nearly constant, whereas it increases for InAlN by 21%, if the composition is changed from $x = 0$–0.5. The increase of the dielectric coefficient is much more pronounced, if Al atoms of wurtzite AlN are replaced by Sc atoms. We observe a nonlinear enhancement by 235% over the same range of compound composition. For convenience, we have approximated the experimental

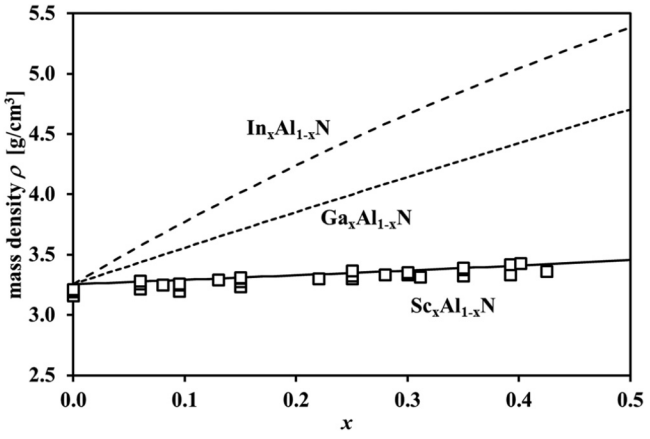

FIG. 4. Measured (open squares) and calculated density of $\mathrm{Sc}_x\mathrm{Al}_{1-x}\mathrm{N}$ (solid line) vs alloy composition x.[24] The values for $\mathrm{Ga}_x\mathrm{Al}_{1-x}\mathrm{N}$ and $\mathrm{In}_x\mathrm{Al}_{1-x}\mathrm{N}$ (dashed lines from Ref. 19) are shown for comparison.

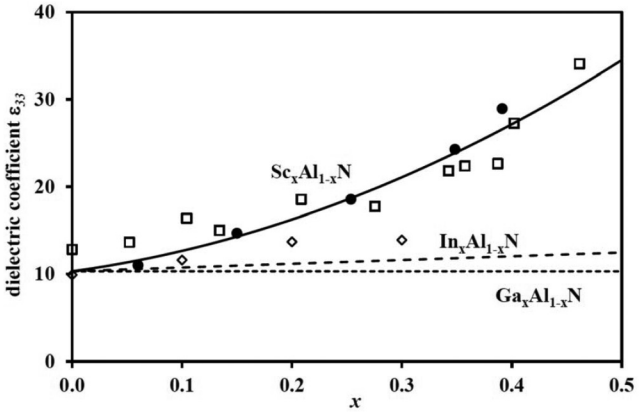

FIG. 5. Measured (symbols: open squares,[9] black circles,[24] and open rhombus[30]) and calculated dielectric coefficient ε_{33} of $Sc_xAl_{1-x}N$ [solid line, Eq. (8)] vs alloy composition x. The values for $Ga_xAl_{1-x}N$ and $In_xAl_{1-x}N$ (dashed lines) are shown for comparison.[19,33]

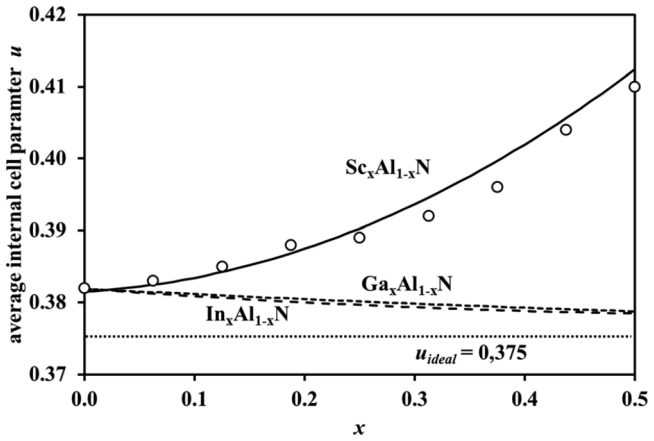

FIG. 6. Calculated (symbols: open circles[10]) average internal cell parameter u depending on alloy composition of $Sc_xAl_{1-x}N$. The dependencies $u(x)$ for $Ga_xAl_{1-x}N$ and $In_xAl_{1-x}N$[19,34,35] are shown for comparison.

results obtained for $\varepsilon_{33}^{ScAlN}(x)$ by a quadratic equation,

$$\varepsilon_{33}^{\mathrm{ScAlN}}(x) = 89.93x + 10.31(1-x) - 62.48\,x\,(1-x), \tag{8}$$

which is in good agreement with the results of Refs. 9 and 31. In order to understand the nonlinearities observed as well as to clarify the cause for the deviation of $\varepsilon_{33}(x)$, $\rho(x)$, and $c(x)/a(x)$ of unstrained ScAlN crystals from the values expected for ideal wurtzite crystals, we calculated the average distances between next nearest and second nearest neighbor atoms as well as the average bond angles and bond length for random wurtzite MeAlN alloys.[10,19] For this purpose, we determine two types of average first neighbor metal–nitrogen bond distances: Me–N_c along the c axis (one bond) and Me–N_b in the basal plane (three bonds),

$$\mathrm{Me} - \mathrm{N}_{c1} = uc, \tag{9}$$

$$\mathrm{Me} - \mathrm{N}_{b1} = \sqrt{\frac{1}{3}a^2 + \left(\frac{1}{2} - u\right)^2 c^2}, \tag{10}$$

as well as two average bond angles $\alpha = \angle(\mathrm{Me–N}_{c1};\ \mathrm{Me–N}_{b1})$, $\beta = \angle(\mathrm{Me–N}_{b1};\ \mathrm{Me–N}_{b'1})$,

$$\alpha = \frac{\pi}{2} + \arccos\left\{\left(\sqrt{1 + 3\left(\frac{c}{a}\right)^2\left(\frac{1}{2} - u\right)^2}\right)^{-1}\right\},$$
$$\beta = 2\arcsin\left\{\left(\sqrt{\frac{4}{3} + 4\left(\frac{c}{a}\right)^2\left(\frac{1}{2} - u\right)^2}\right)^{-1}\right\}, \tag{11}$$

where u denotes the cell-internal parameter (see Fig. 6–11). In addition, three types of average second neighbor metal–nitrogen distances,

$$\mathrm{Me} - \mathrm{N}_{c2} = (1-u)c, \tag{12}$$

$$\mathrm{Me} - \mathrm{N}_{b2} = \sqrt{a^2 + (uc)^2}, \tag{13}$$

$$\mathrm{Me} - \mathrm{N}_{b'2} = \sqrt{\frac{4}{3}a^2 + \left(\frac{1}{2} - u\right)^2 c^2}, \tag{14}$$

as well as second neighbor metal–metal Me–M_c and Me–M_b distances have been calculated. In Eqs. (9)–(14), we neglect the tilt of the Me–N_c bond against the c axis which is increasing with Sc

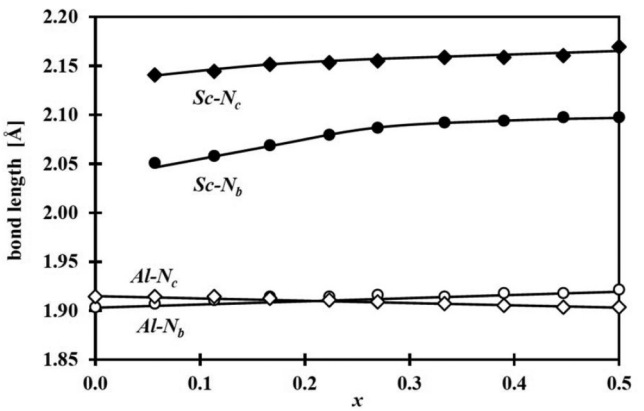

FIG. 7. Calculated average bond length between nearest neighbor metal and nitrogen atoms oriented along the c axis (M–N_c) or in the basal plane (M–N_b) for ScAlN with x of up to 0.5. Beside a higher bond length, the Sc–N bonds show a significant dependence on orientation.

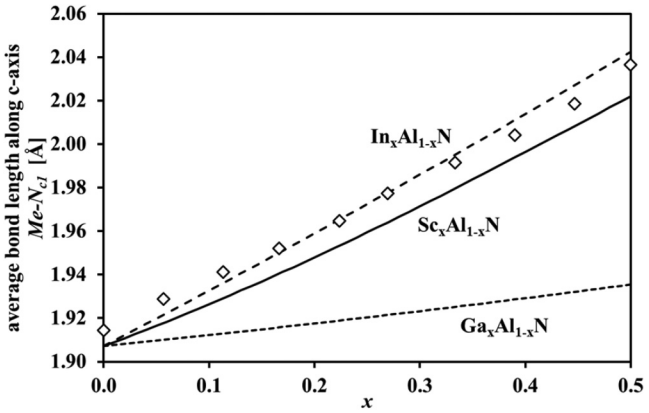

FIG. 8. Average bond length of metal and nitrogen atoms oriented along the *c* axis (M–N_c) vs metal atom concentration x for $Me_xA_{1-x}N$ (Me = Ga, In, or Sc) calculated by Eqs. (9)–(14). The rhombohedral symbols are results of DFT simulations for $Sc_xA_{1-x}N$.[10]

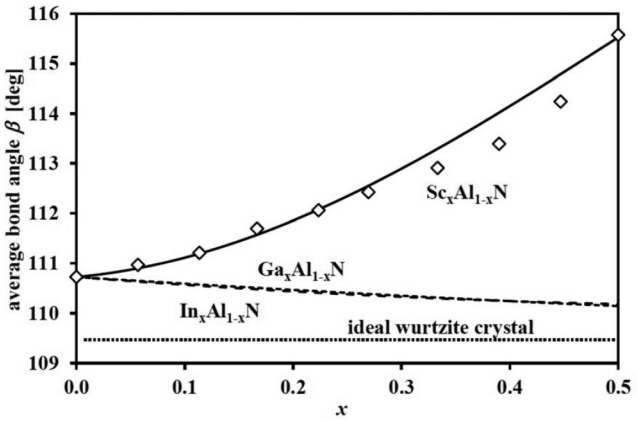

FIG. 10. Average bond angle β vs metal atom concentration x for $Me_xAl_{1-x}N$ (Me = Ga, In, or Sc) calculated by Eqs. (9)–(14). The rhombohedral symbols are results of DFT simulations for $Sc_xA_{1-x}N$.[10]

incorporation up to 3.5° for $x = 0.5$. This effect is included in our DFT simulations and discussed in more detail in Ref. 10. It should be noticed that in the case of an ideal wurtzite crystal, the ratio of lattice parameters,

$$\frac{c}{a} = \sqrt{\frac{8}{3}} = 1.633, \tag{15a}$$

and ideal cell-internal parameter,

$$u = \frac{3}{8} = 0.375, \tag{15b}$$

is defined by Eqs. (15a) and (15b), and in consequence, it follows that the bond length and the bond angles between the nearest neighbors ($\alpha = \beta = 109.47°$) are equal but the distance to the second nearest neighbor along the *c* axis is about 13% shorter than the distance to the second nearest neighbors in the basal plane (this is not the case in the cubic structure).[32] It is known from experiment as well as theoretical predictions that neither the cell-internal parameter u nor the c/a-ratio is ideal in wurtzite group-III-nitrides.[19,33,34] In order to understand the non-ideality of the wurtzite structure and its polarization and mechanical properties, we have calculated the average bond lengths and angles as well as the second neighbor distances (virtual crystal limit) of random ternary alloys taking advantage of the lattice constants and the calculated average u parameter. The average cell-internal parameter is defined as the average value of the projection of the connecting vector pointing from a nitrogen to its nearest neighbor metal atom in the [0001] direction. The quadratic equations (16a) and (16b) describing $u(x)$

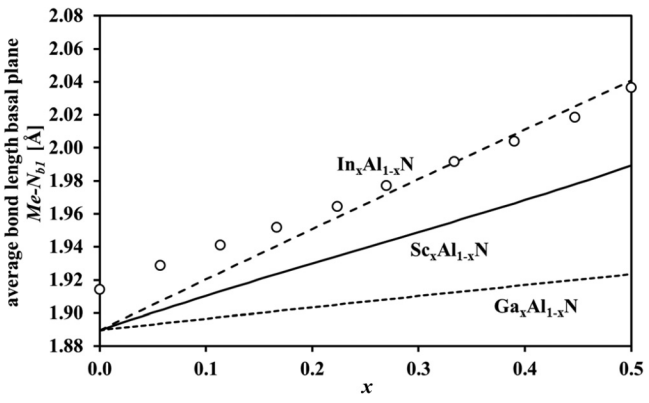

FIG. 9. Average bond length of metal and nitrogen atoms oriented along the basal plane (M–N_b) vs metal atom concentration x for $Me_xA_{1-x}N$ (Me = Ga, In, or Sc) calculated by Eqs. (9)–(14). The open circles are results of DFT simulations for $Sc_xA_{1-x}N$.[10]

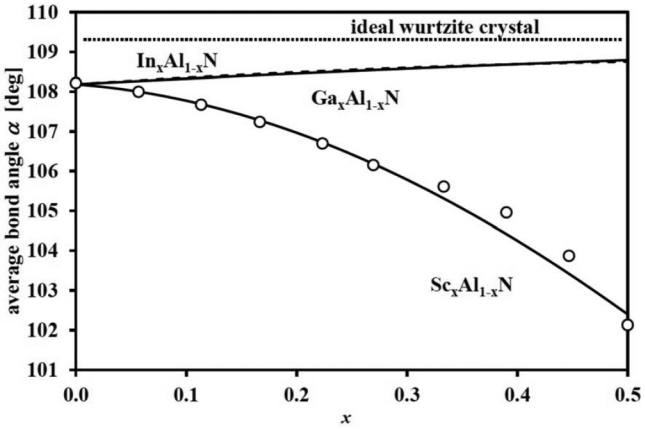

FIG. 11. Average bond angle α vs metal atom concentration x for $Me_xAl_{1-x}N$ (Me = Ga, In, or Sc) calculated by Eqs. (9)–(14). The open circles are results of DFT simulations for $Sc_xA_{1-x}N$.[10]

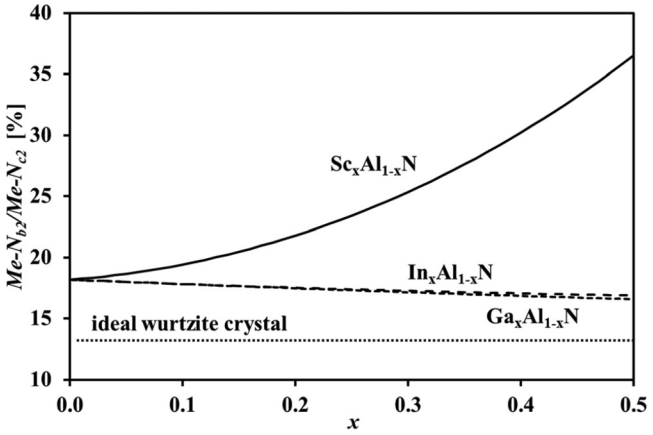

FIG. 12. Ratio r of second nearest neighbor Me–N distances oriented along the c axis or located in the basal plane vs metal atom concentration x for $Me_xAl_{1-x}N$ (Me = Ga, In, or Sc) calculated by Eq. (17) using Eqs. (9)–(14).

for $Ga_xAl_{1-x}N$ and $In_xAl_{1-x}N$ are provided by Refs. 19 and 33–36. The quadratic equations (16c) describing $u^{ScAlN}(x)$ is an approximation to the data simulated by Urban *et al.*,[10] rescaled to the u parameter of AlN,[19]

$$u^{GaAlN}(x) = 0.3772\,x + 0.3819\,(1-x) - 0.0032\,x\,(1-x), \quad (16a)$$

$$u^{InAlN}(x) = 0.3793\,x + 0.3819\,(1-x) - 0.0086\,x\,(1-x), \quad (16b)$$

$$u^{ScAlN}(x) = 0.4967\,x + 0.3815\,(1-x) - 0.1068\,x\,(1-x). \quad (16c)$$

The nonlinear dependences of the average cell-internal parameters on alloy composition are described by negative bowing

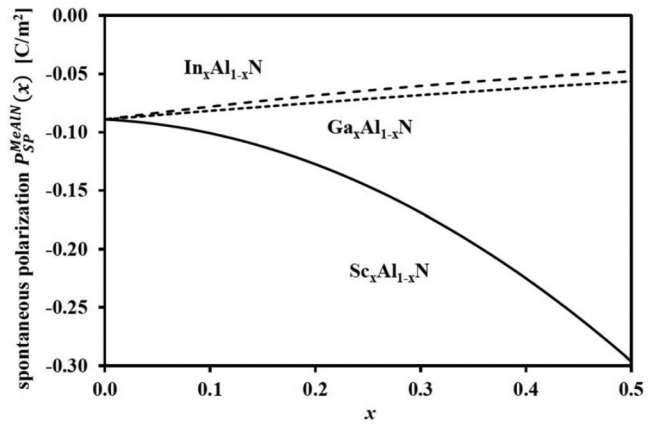

FIG. 13. Spontaneous polarization vs metal atom concentration x for metal polar, random $Me_xAl_{1-x}N$ (Me = Ga, In, or Sc) alloys with wurtzite crystal structure [Eq. (18)].

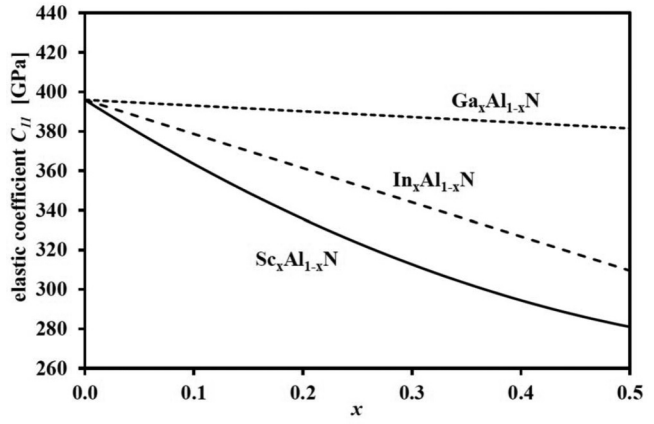

FIG. 14. Calculated elastic coefficient C_{11} vs metal atom concentration x for $Sc_xAl_{1-x}N$ alloys with the wurtzite crystal structure [solid line, Eq. (23a)[10]]. The linear interpolation between the two relevant binary nitrides for $Ga_xAl_{1-x}N$ and $In_xAl_{1-x}N$ (dashed lines) are shown for comparison.[19]

parameters, which values increase from GaAlN to InAlN to ScAlN. It should be pointed out that although the bowing parameters are negative, the average cell-internal parameter of random alloys investigated is always above the ideal value ($u_{MeAlN} > u_{ideal} = 0.375$) indicating elongated bonds (Fig. 6). Except the Al–N_c bonds, the nearest neighbor Al–N and Sc–N as well as Al–Al and Sc–Al distances, calculated by our DFT approach for ScAlN, increase as a function of alloy composition ($0 \le x \le 0.5$). Beside the expected larger bond length of Sc–N in comparison to Al–N, it becomes obvious by looking at Fig. 7 that the distance of nearest neighbor Sc–N atoms oriented along the c axis is significant larger in comparison to the distances determined for bonds oriented along the basal plane.

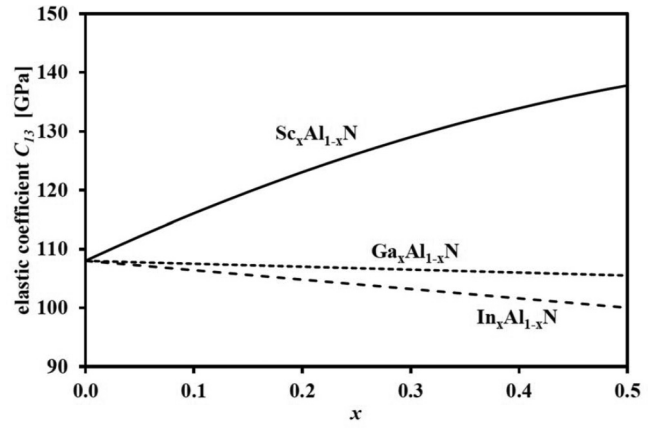

FIG. 15. Calculated elastic coefficient C_{13} vs metal atom concentration x for $Sc_xAl_{1-x}N$ alloys with the wurtzite crystal structure (solid line). The linear interpolation between the two relevant binary nitrides for $Ga_xAl_{1-x}N$ and $In_xAl_{1-x}N$ (dashed lines) are shown for comparison.[19]

As a consequence, the Al–N_3 and even more significant the Sc–N_3 tetrahedrons are elongated along the c axis in comparison to the tetrahedrons of an ideal wurtzite structure. Because the Sc–N bonds are about 8% and 12% longer in comparison to the Al–N bonds oriented along the basal plane and c axis, respectively, the local strain field caused by Sc hinders the incorporation of an additional Sc atom on the nearest neighbor position suitable for a metal atom in ScAlN. This results in difficulties to achieve high Sc-concentration alloys at crystal growth conditions close to thermal equilibrium and causes a high surface diffusion length of Sc atoms during crystal growth.

In order to follow the trend of changes in structural properties toward higher alloy compositions, the average bond lengths and angles are determined from our DFT simulations and by using Eqs. (9)–(14). The average metal–nitrogen distances increase nearly linearly with alloy composition for GaAlN, InAlN, and ScAlN. Only the average scandium–nitrogen length for bonds oriented along the c axis shows a slight bowing. The values of the average metal–nitrogen bond length calculated by Eqs. (9)–(14) for ScAlN are between the bond lengths of GaAlN and InAlN (Figs. 8 and 9). The values of the average Sc–N bonds simulated by DFT are 0.4%–1.1% larger in comparison to results of Eqs. (9)–(14). For GaAlN and InAlN, the average angles α and β between Me–N bonds approaching the ideal bond angle $\alpha_{\text{ideal}} = 109.47°$ (Figs. 10 and 11), if an increasing number of Al atoms are replaced by Ga or In. If Al atoms are substituted by Sc, the bond angles deviate more and more from the ideal value, indicating an increasing elongation of the Me–N_3 tetrahedrons in direction of the c axis for ScAlN with increasing Sc content. The ratio r^{AlN} of the average distances to the second nearest neighbors along the c axis (Me–N_{c2}) and along the basal plane (Me–N_{b2}, Me–$N_{b'2}$) for AlN is well above the ratio of the ideal wurtzite structure (r^{ideal}),

$$r^{\text{AlN}} = \left(1 - \frac{\text{Me} - \text{N}_{c2}}{\text{Me} - \text{N}_{b2}}\right)100\% = 18\% > 13\% = r^{\text{ideal}}, \qquad (17)$$

and decreases slightly nonlinear, if Al atoms are substituted by Ga or In (Fig. 12). In opposite to GaAlN and InAlN, for ScAlN, the ratio is increasing nonlinear up to 36.5%, if half of the Al atoms are replaced by Sc. Based on these results, it can be summarized that for all random ternary alloys investigated, the wurtzite crystals behave very much like ideal hexagonal crystal lattices whose basal planes are under biaxial compressive stress, whereas this virtual stress is relaxed if Al atoms are replaced by an increasing number of Ga or In atoms, it is strongly enlarged by incorporation of Sc into the crystal lattice. Beside the significant deviation of ScAlN from the ideal wurtzite structure, it should be noticed that the observed nonlinearity in the average cell-internal parameter, the second neighbor atom distances as well as bond angels of the random alloys always tend to decrease the differences between the "real" and ideal wurtzite crystal structures. Nevertheless, because of the polar nature of the Me–N bonds, the missing inversion symmetry of the (ideal) wurtzite lattice and on top of this, the observed elongation of the Me–N_3 tetrahedrons along the c axis, the ternary alloys investigated will show spontaneous polarization, which will be discussed in more detail below.

IV. SPONTANEOUS POLARIZATION

Computational studies of spontaneous polarization and piezoelectricity of random alloys with the wurtzite structure in GaAlN and InAlN have been performed by Bernardini *et al.*[36] for GaAlN and InAlN and carried out for ScAlN by Caro *et al.*[37] The simulations are based on DFT and the Berry-phase theory[38,39] using periodic supercells. To determine the polarization Bernardini has chosen centrosymmetric (unstrained) zinc blende lattices as reference states. The ideal wurtzite structure served in order to obtain the offset corrections to electronic and ionic polarizations. The evolution of the polarization from ideal to the real (relaxed) wurtzite structures gives the value of the spontaneous polarization. The variation of the polarization upon deformations of the relaxed structures enables the calculation of the piezoelectric tensor (Chap. VI). Caro *et al.*[37] have constructed ideal wurtzite supercells which can lead to straight-forward polarization offsets and the calculation of the zinc blende reference structure can be skipped. It should be mentioned that Dreyer *et al.*[40] recommend a stacked hexagonal instead of a zinc blende structure as reference for the calculation of polarization in order to avoid a nonzero polarization in the [111] direction. This polarization can be significant and occurs, if the in-plane lattice constant of the zinc blende reference is adapted to the corresponding wurtzite crystal. The significance of this effect on the comparison of the spontaneous polarization of InAlN, GaAlN, and ScAlN carried out here is the subject of ongoing simulations. Due to the good agreement between the simulated and the measured piezoelectric polarizations (Chap. 6), we use the data from Bernardini *et al.* and Caro *et al.* for further discussions.

It has been predicted by theory and confirmed by experiment that GaAlN and InAlN alloys having the wurtzite crystal structure show large values of polarizations[33–35] varying nonlinear with composition x. Zoroddu *et al.* pointed out earlier that the spontaneous polarization of unstrained alloys for a given composition depends linearly on the average internal cell parameter u which indicates spontaneous polarization differences between alloys of the same composition are mainly due to varying metal nitrogen bond length.[33] This idea is supported by the fact that in binaries the polarization is strongly influenced by the relative displacement of the cation and anion sublattices in the [0001]-direction.[34,35] Beside the nonlinearities, caused by the structural properties, Bernardini *et al.*[36] proved that the different cation electronegativities contribute significantly to the nonlinear behavior of spontaneous polarization in ternary random alloys. The nonlinear spontaneous polarization, oriented in [0001]-direction, predicted by Bernardini and Caro *et al.*,[36,37] taken the structural and electronegativity effects into account, can be approximated by (in C/m^2),

$$P_{\text{SP}}^{\text{GaAlN}}(x) = -0.034\,x - 0.090\,(1-x) + 0.019\,x\,(1-x), \qquad (18a)$$

$$P_{\text{SP}}^{\text{InAlN}}(x) = -0.042\,x - 0.090\,(1-x) + 0.071\,x\,(1-x), \qquad (18b)$$

$$P_{\text{SP}}^{\text{ScAlN}}(x) = -0.874\,x - 0.089\,(1-x) + 0.741\,x\,(1-x), \qquad (18c)$$

for random, metal polar GaAlN, InAlN, and ScAlN alloys (see also Fig. 13). For nitrogen polar alloys, the sign of the spontaneous

polarization has to be changed from minus to plus. As expected from the variation in the internal cell parameter with alloy composition, the value of spontaneous polarization decreases, if Al atoms are replaced by Ga or In, whereas the value of spontaneous polarization is largely enhanced if Al is substituted by Sc atoms. It should be pointed out that for the whole range of alloy compositions investigated the values of spontaneous polarization of ScAlN are exceeding the values of GaAlN and InAlN. A moderate bowing is calculated for GaAlN, which is enlarged for InAlN due to the differences of the dynamical charges of Al–N, Ga–N, and In–N bonds, determined to be 2.653, 2.670, and 3.105, respectively.[33–35] The predicted bowing parameter of the spontaneous polarization for ScAlN is an order of magnitude higher in comparison to InAlN, mainly due to the strong nonlinear dependence of the internal cell parameter vs Sc concentration (Fig. 6). It becomes obvious that nonlinear effects have to be taken into account, if structural and polarization related properties of ScAlN are described in dependence on alloy composition.

In the case of polarization related effects, the knowledge of the spontaneous polarization is not sufficient to predict, e.g., polarization induced surface and interface charges as well as resulting electric fields in strained ScAlN crystals. Crystals with spontaneous polarization show piezoelectric polarization if external forces or electric fields are applied. To take these effects into account, the mechanical properties and piezoelectric coefficients of ScAlN are discussed and compared to GaAlN and InAlN in the next chapter.

V. MECHANICAL PROPERTIES

The deformation of a crystal ε_{kl} due to external or internal forces or stresses σ_{ij} can be described by Hook's law,

$$\sigma_{ij} = \sum_{k,l} C_{ijkl}\varepsilon_{kl}, \tag{19}$$

where C_{ijkl} is the elastic tensor. Due to spacial symmetry, this fourth rank tensor can be reduced to a 6×6 matrix using the Voigt notation: xx → 1, yy → 2, zz → 3, yz, zy → 4, zx, xz → 5, and xy, yx → 6. The elements of the elastic tensor can be rewritten as $C_{ijkl} = C_{mn}$ were i, j, k, l = x, y, and z and m, n = 1,…, 6. Using this notation, Hook's law can be simplified to

$$\sigma_i = \sum_j C_{ij}\varepsilon_j. \tag{20}$$

The 6×6 matrix of the elastic constants C_{ij} for crystals with the wurtzite structure is given by[41]

$$C_{ij} = \begin{pmatrix} C_{11} & C_{12} & C_{13} & 0 & 0 & 0 \\ C_{12} & C_{11} & C_{13} & 0 & 0 & 0 \\ C_{13} & C_{13} & C_{33} & 0 & 0 & 0 \\ 0 & 0 & 0 & C_{44} & 0 & 0 \\ 0 & 0 & 0 & 0 & C_{44} & 0 \\ 0 & 0 & 0 & 0 & 0 & \frac{1}{2}(C_{11}-C_{12}) \end{pmatrix}. \tag{21}$$

The elastic constants have been calculated by Zhang *et al.*[17] for wurtzite $Sc_xAl_{1-x}N$ alloys up to $x = 0.375$. The crystals were first fully relaxed using density functional theory (DFT).[42] Then, the Vienna *Ab initio* Simulation Package (VASP) was used for structural optimization, using the generalized gradient approximation (GGA) as parameterized by Perdew *et al.*[43] for the exchange-correlation potential. Projector augmented wave basis sets were employed in VASP calculations with a plane wave cutoff of 450 eV. This cutoff value was chosen to retain consistency with previous calculations[17] to achieve reasonable computational times and to offset the known underestimation of elastic constants usually associated with the use of the Perdew–Burke–Ernzerhof functional. The simulation supercells were constructed using the special quasi-random structure methodology to best represent a random alloy using 32 and 128-atom supercells. The elastic coefficients calculated have been approximated by linear dependences on Sc concentration (in GPa),

$$C_{11}^{\mathrm{ScAlN}}(x) = -262.7\,x + 389.5, \tag{22a}$$

$$C_{12}^{\mathrm{ScAlN}}(x) = 24.8\,x + 13.8, \tag{22b}$$

$$C_{13}^{\mathrm{ScAlN}}(x) = 62.1\,x + 108.2, \tag{22c}$$

$$C_{33}^{\mathrm{ScAlN}}(x) = -459.2\,x + 364.6, \tag{22d}$$

$$C_{44}^{\mathrm{ScAlN}}(x) = -50.4\,x + 116.0. \tag{22e}$$

As described in Chap. II, we have used a very similar approach to Zhang[17] and Caro.[37] The elastic constants calculated using GGA are known to be slightly underestimated for III-nitrides due to the "under-binding."[44] However, the trends in elastic constants predicted by Zhang or Caro and our approach are very comparable. We have, thus, retained the GGA approach and adjusted the absolute values of the elastic constants for $x = 0$ so that they are in agreement with previous data determined experimentally and theoretically for AlN.[41,45–47] To be consisted with the observed nonlinear behavior of structural properties of $Sc_xAl_{1-x}N$ ($0 \le x \le 0.5$), we have chosen quadratic equations to approximate the DFT simulated values for the elastic coefficients (in GPa),

$$C_{11}^{\mathrm{ScAlN}}(x) = 285.12\,x + 396.00\,(1-x) - 238.39\,x\,(1-x), \tag{23a}$$

$$C_{12}^{\mathrm{ScAlN}}(x) = 180.57\,x + 137.00\,(1-x) + 11.23\,x\,(1-x), \tag{23b}$$

$$C_{13}^{\mathrm{ScAlN}}(x) = 141.70\,x + 108.00\,(1-x) + 51.95\,x\,(1-x), \tag{23c}$$

$$C_{33}^{\mathrm{ScAlN}}(x) = -155.17\,x + 373.00\,(1-x) + 95.49\,x\,(1-x), \tag{23d}$$

$$C_{44}^{\mathrm{ScAlN}}(x) = 176.44\,x + 116.00\,(1-x) - 158.80\,x\,(1-x). \tag{23e}$$

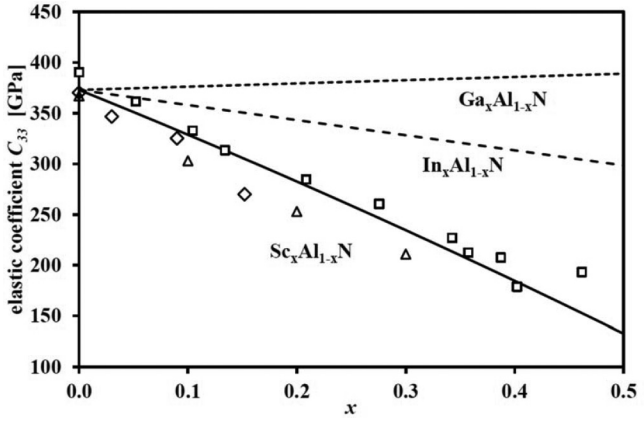

FIG. 16. Calculated elastic coefficient C_{33} vs metal atom concentration x for $Sc_xAl_{1-x}N$ alloys with the wurtzite crystal structure (solid line). The linear interpolation between the two relevant binary nitrides for $Ga_xAl_{1-x}N$ and $In_xAl_{1-x}N$ (dashed lines) are shown for comparison.[19] Open symbols are experimental data taken from the literature (open squares,[9] open triangles,[30] and open rhombs[48]).

In good agreement with the data provided by Zhang *et al.*[17] (Figs. 14–16) and in the case of C_{33} also with experimental results (Fig. 16, Refs. 9, 30, and 48), we observe a decrease of C_{11}, C_{33}, and C_{44} as well as an increase of C_{12} and C_{13} if a growing number of Al atoms is substituted by Sc. In contrast to Zhang *et al.*, we predict a significant nonlinear dependence of C_{11} and C_{44} on alloy composition, which has to be taken into account, e.g., for a precise design of piezo-acoustic devices, whereas the elastic coefficients C_{12} and C_{13} of $Ga_xAl_{1-x}N$ and $In_xAl_{1-x}N$ are decreasing with increasing Ga

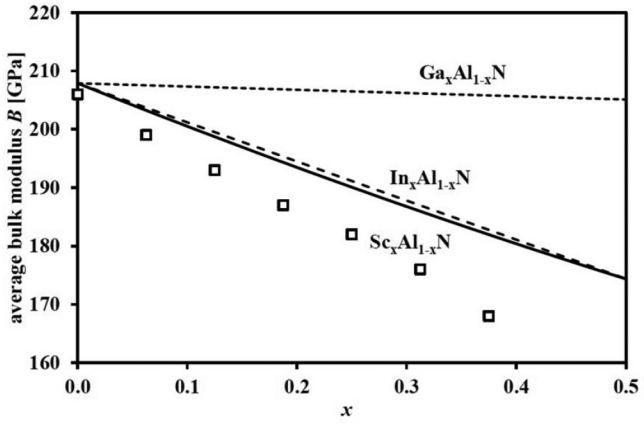

FIG. 17. Calculated average bulk modulus B vs metal atom concentration x for $Sc_xAl_{1-x}N$ alloys with the wurtzite crystal structure [solid line, Eq. (24), DFT data from Ref. 10]. The linear interpolation between the two relevant binary nitrides for $Ga_xAl_{1-x}N$ and $In_xAl_{1-x}N$ (dashed lines from Ref. 19) are provided for comparison.

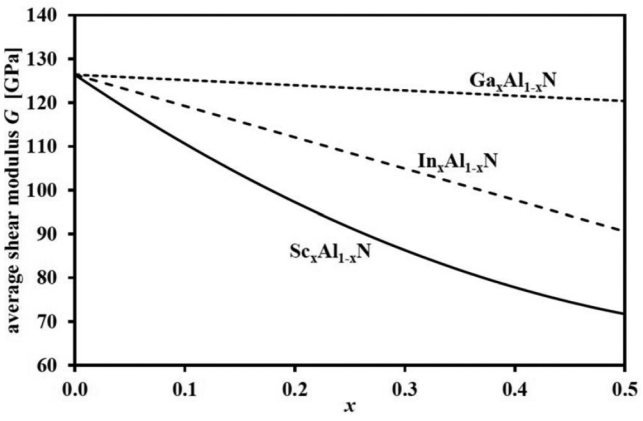

FIG. 18. Calculated average shear modulus G vs metal atom concentration x for $Sc_xAl_{1-x}N$ alloys with the wurtzite crystal structure [solid line, Eq. (25)]. The linear interpolation between the two relevant binary nitrides for $Ga_xAl_{1-x}N$ and $In_xAl_{1-x}N$ (dashed lines) are shown for comparison.

or In content, these coefficients are enlarged by adding Sc to the AlN lattice, indicating an inhomogeneous softening of the hexagonal lattice as discussed in more detail in the following. The elastic quantities of $Sc_xAl_{1-x}N$, such as the average bulk modulus B, shear modulus G, and the Young modulus E, were derived from the set of elastic constants listed above [Eqs. (23a)–(23e)] using the following equations:[49–51]

$$B = \frac{1}{9}(2C_{11} + 2C_{12} + 4C_{13} + C_{33}), \tag{24}$$

$$G = \frac{1}{30}(C_{11} + C_{12} + 2C_{33} - 4C_{13} + 12C_{44} + 12C_{66}), \tag{25}$$

$$E = \frac{9BG}{3B + G}. \tag{26}$$

For convenience, these physical properties have been approximated by the following quadratic equations (in units of GPa):

$$B^{\mathrm{ScAlN}}(x) = 149.0\,x + 208.0\,(1-x) - 18\,x\,(1-x), \tag{27}$$

$$G^{\mathrm{ScAlN}}(x) = 77.8\,x + 126.4\,(1-x) - 121.6\,x\,(1-x), \tag{28}$$

$$E^{\mathrm{ScAlN}}(x) = 198.8\,x + 315.4\,(1-x) - 271.6\,x\,(1-x) \tag{29}$$

and compared to data taken from the literature.[52] It becomes obvious from Figs. 17–19 and Eqs. (27)–(29) that $Sc_xAl_{1-x}N$ becomes softer with increasing x, similar to $In_xAl_{1-x}N$, but more pronounced. The trends observed for the average bulk modulus B, shear modulus G, and the Young modulus E are associated with three factors specific to ScAlN. First, an increasing deviation away from ideal tetrahedral bonding (increased value of internal cell parameter) occurs with increasing x. Second, the average bond

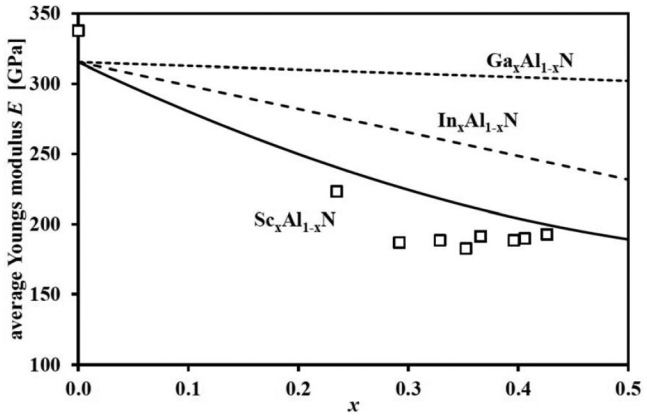

FIG. 19. Calculated average Young's modulus E vs metal atom concentration x for $Sc_xAl_{1-x}N$ alloys with the wurtzite crystal structure [solid line, Eq. (26)]. The values measured (open squares[52]) as well as the ones for $Ga_xAl_{1-x}N$ and $In_xAl_{1-x}N$ (dashed lines) are shown for comparison.

lengths and in-plane lattice parameters increase with enhanced Sc content, a trend which is associated with a reduction in B, G, and E in all the common wurtzite structure semiconductors.[53] Third, the average bond ionicity increases with increasing Sc content, which is expected given the higher ionicity of Sc–N bonding in ScN compared to Ga–N and Al–N bonding in GaN and AlN. This observation is confirmed by DFT computations, which indicate a higher electron density surrounding the N atoms adjacent to a Sc atom than the N atoms adjacent only to Ga or Al atoms. It should be noticed that increasing bond ionicity is already known to lead to a reduction in the shear moduli in tetrahedral coordinated semiconductors.[54] In addition to the elastic coefficients, a useful way to describe the mechanical properties in dependence of orientations within ScAlN crystals are the elastic compliance coefficients. If the piezoelectric effect is neglected, the compliance matrix corresponds to the inverse of the elasticity matrix, taking advantage of the elastic constants described by the set of Eqs. (23a)–(23e) and using the following relations:

$$S_{11} = \frac{C_{11}C_{33} - C_{13}^2}{(C_{11} - C_{12})[C_{33}(C_{11} + C_{12}) - 2C_{13}^2]}, \tag{30a}$$

$$S_{12} = -\frac{C_{12}C_{33} - C_{13}^2}{(C_{11} - C_{12})[C_{33}(C_{11} + C_{12}) - 2C_{13}^2]}, \tag{30b}$$

$$S_{13} = -\frac{C_{13}}{C_{33}(C_{11} + C_{12}) - 2C_{13}^2}, \tag{30c}$$

$$S_{33} = \frac{C_{11} + C_{12}}{C_{33}(C_{11} + C_{12}) - 2C_{13}^2}, \text{ and} \tag{30d}$$

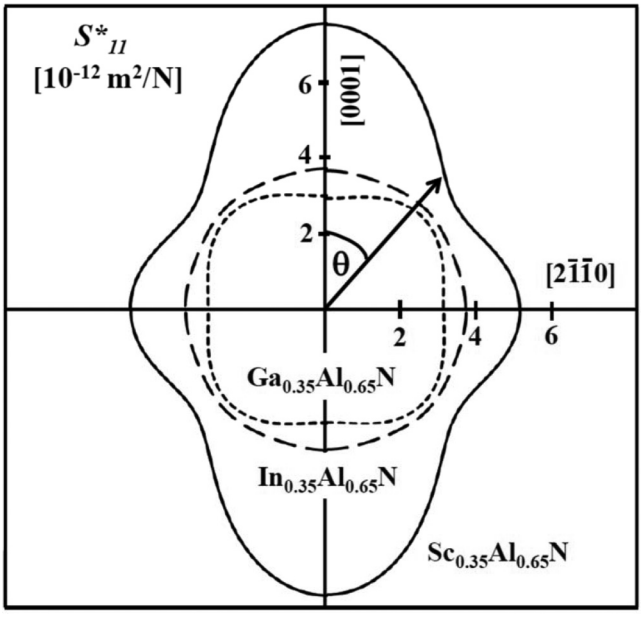

FIG. 20. Reciprocal Young's modulus S_{11}^* in dependence on the angle Θ with respect to the c axis for $Sc_{0.35}Al_{0.65}N$ [solid line, Eq. (31)] and $Ga_{0.35}Al_{0.65}N$ and $In_{0.35}Al_{0.65}N$ (dashed lines[19]).

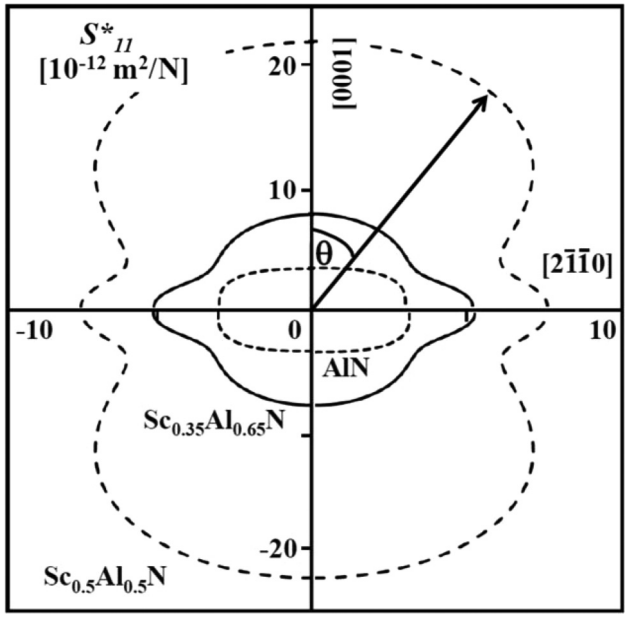

FIG. 21. Reciprocal Young's S_{11}^* modulus in dependence on the angle Θ with respect to the c axis for AlN (inner dashed line), $Sc_{0.35}Al_{0.65}N$ (solid line), and $Sc_{0.5}Al_{0.5}N$ (outer dashed line).

$$S_{44} = \frac{1}{C_{44}}. \tag{30e}$$

Using these compliance coefficients, a helpful figure of merit to determine the directional stiffness, the reciprocal Young's modulus as a function of orientation to the crystal axis can be provided. For hexagonal materials, the reciprocal Young's modulus S_{11}^{*} at an angle Θ with respect to the [0001]-axis is given by[55]

$$S_{11}^{*}(\theta) = S_{11}\sin^4(\theta) + S_{33}\cos^4(\theta) + (S_{44} + 2S_{13})\sin^2(\theta)\cos^2(\theta). \tag{31}$$

Figure 20 shows $S_{11}^{*}(\theta)$ for $Me_{0.35}Al_{0.65}N$ (Me = Ga, In, or Sc) as a function of direction with respect to the [0001]-axis. The closer the position of $S_{11}^{*}(\theta)$ is located to the origin of the polar plot, the "stiffer" the crystal responds to an external force applied at an angle θ with respect to the [0001]-axis. It is seen that for all angles θ, the substitution of Al atoms by Sc in wurtzite AlN is softening the crystal more significant in comparison to a substitution by In and Ga. Looking into the polar profile of $S_{11}^{*}(\theta)$ in more detail, it can be noticed that the stiffness of $In_{0.35}Al_{0.65}N$ is isotropic ($S_{11}^{*}(\theta) = (3.68 \pm 0.03)\mathrm{m^2\,N^{-1}}$) in the (0001)/(2$\bar{1}\bar{1}$0)-plane, whereas $Ga_{0.35}Al_{0.65}N$ shows a pronounced softening by $\Delta S_{11}^{*}(\theta = 47°) = (0.5 \pm 0.1) \times 10^{-12}\ \mathrm{m^2\,N^{-1}}$ in comparison to the stiffness along the [0001]- and [2$\bar{1}\bar{1}$0]-axes. The reciprocal Young's modulus of $Sc_{0.35}Al_{0.65}N$ is not isotropic; it is about 30% larger along the [0001] in comparison to the [2$\bar{1}\bar{1}$0]-axis. Furthermore, the highest stiffness is observed at an angle of 55° ($S_{11}^{*}(\theta = 55°) = 4.33 \times 10^{-12}\ \mathrm{m^2\,N^{-1}}$). As can be seen from Fig. 21, the anisotropic behavior of wurtzite ScAlN is enlarged by increased Sc content. At $x = 0.5$, we have calculated the reciprocal Young's modulus $S_{11}^{*}(\theta = 0°) = 21.31 \times 10^{-12}\ \mathrm{m^2\,N^{-1}}$ to be three times higher in comparison to $S_{11}^{*}(\theta = 90°)$ and the angle of highest stiffness is found to be at $\theta = 65°$. For AlN, we observe the highest stiffness (lowest $S_{11}^{*}(\theta) = (3.01 \pm 0.02) \times 10^{-12}\ \mathrm{m^2\,N^{-1}}$) along the [0001]- and [2$\bar{1}\bar{1}$0]-axes and the angle of highest reciprocal Young's modulus at $\theta = 45°$. It becomes obvious that the angular dependent mechanical properties of ScAlN in the (0001)/(2$\bar{1}\bar{1}$0)-plane are completely different to binary AlN, which can be relevant for the design of ScAlN-based piezoelectric and micromechanical devices.

The observation of the anisotropic reciprocal Young's modulus of wurtzite ScAlN and its relevance for piezo-acoustic devices motivates the investigation of the Poisson ratios. The Poisson ratio, ν, is defined for isotropic media as the quotient of lateral contraction to longitudinal extension arising from application of tensile stress. The ratio finds application in a number of areas of applied elasticity and solid mechanics, for example, as an indication of the mechanical coupling between various vibrational modes of motion. Poisson's ratio for crystals is related to the elastic compliance coefficients and defined in general as

$$\nu_{ji} = -\frac{S_{ij}}{S_{jj}}, \tag{32}$$

where x_j is the direction of the uniaxial longitudinal extension, x_i is the direction of the accompanying lateral contraction, and the S_{ij} and S_{jj} are the appropriate elastic compliances.[56] The application of the definition requires specification of the orientation of the x_k coordinate set with respect to the crystallographic directions and transformation of the compliances accordingly. For now, the influence of piezoelectricity on the Poisson ratios is neglected. It suffices to take x_1 as the direction of the longitudinal extension; then, two Poisson ratios are defined by the orientations of the lateral axes x_2 and x_3. For longitudinal uniaxial extension of wurtzite crystals

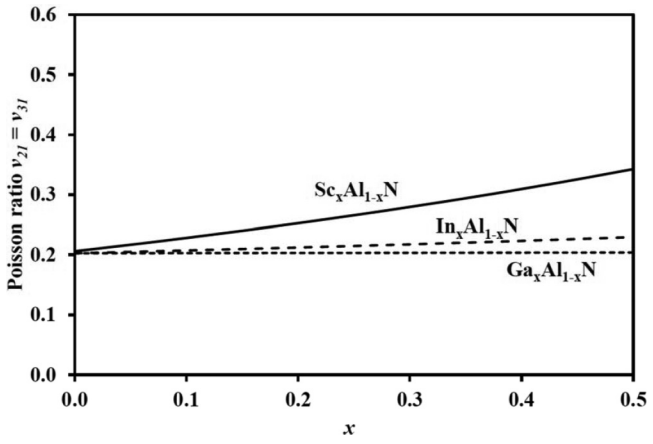

FIG. 22. Calculated Poisson ratio $\nu_{21} = \nu_{31}$ for longitudinal uniaxial extension of wurtzite $Sc_xAl_{1-x}N$ crystals along the [0001]-axis vs metal atom concentration x (solid line). The values for $Ga_xAl_{1-x}N$ and $In_xAl_{1-x}N$ (dashed lines) are provided for comparison.

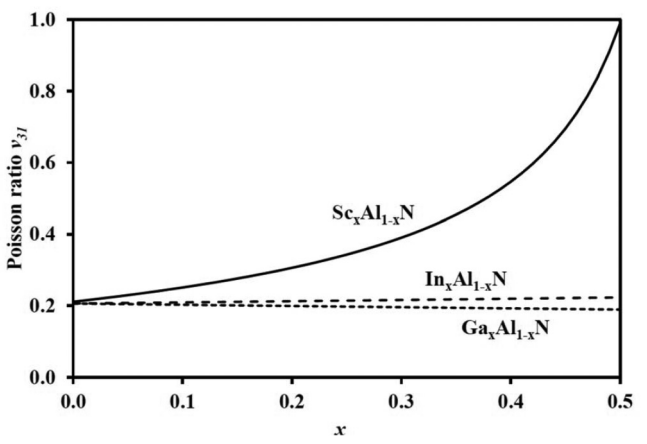

FIG. 23. Calculated Poisson ratio ν_{31} for longitudinal uniaxial extension of wurtzite $Sc_xAl_{1-x}N$ crystals in the basal plane vs metal atom concentration x (solid line). The linear interpolation between the two relevant binary nitrides for $Ga_xAl_{1-x}N$ and $In_xAl_{1-x}N$ (dashed lines) are shown for comparison.

along the [0001]-axis, the Poisson ratios can be described by

$$\nu_{21} = \nu_{31} = -\frac{S_{13}}{S_{33}} \tag{33}$$

and for the longitudinal uniaxial extension in the basal plane by

$$\nu_{21} = -\frac{S_{12}}{S_{11}}, \quad \nu_{31} = -\frac{S_{13}}{S_{11}}. \tag{34}$$

For uniaxial extension along the [0001]-axis, the Poisson ratio of AlN is calculated to $\nu_{21}(x=0) = \nu_{31}(x=0) = 0.206$. By substituting Al atoms by Ga or In, a slight increase [$\nu_{21}(x_{Ga}=0.5) = 0.204$] or decrease [$\nu_{21}(x_{In}=0.5) = 0.230$] of the Poisson ratio is observed, respectively (Fig. 22). If Al is substituted by Sc, a significant increase of the Poisson ratio is determined [$\nu_{21}(x_{Sc}=0.5) = 0.343$]. For uniaxial extension in the basal plane, the Poisson ratio $\nu_{21}(x=0) = 0.290$ is increased to 0.304 and 0.335, whereas $\nu_{31}(x=0) = 0.211$ is changing linear to 0.189 and 0.335, if half of the Al atoms are substituted by Ga and In, respectively. The incorporation of Sc into AlN causes a more pronounced nonlinear change in the Poisson ratios (Figs. 23 and 24). For $x_{Sc} = 0.5$, an enlargement of ν_{31} to 0.989 and at the same time, a reduction of ν_{21} to 0.041 is predicted. It should be noticed that the increase of $\nu_{21}(x)$ for $In_xAl_{1-x}N$ and $Sc_xAl_{1-x}N$ are very similar up to $x \approx 0.3$ but for higher Sc concentrations, a drastic reduction of $\nu_{21}(x)$ is observed. The large deviations of the Poisson ratios of ScAlN in comparison to GaAlN and InAlN are mainly a consequence of the anisotropy of the mechanical stiffness and the softening of AlN caused by the incorporation of Sc. These special mechanical properties of ScAlN will also affect the piezoelectric polarization of the wurtzite structure crystals as described in the next chapter. In the following, we will not restrict our self to the discussion of uniaxial extension, we will also address the more application relevant consequences of biaxial and hydrostatic stresses applied to wurtzite ScAlN crystals.

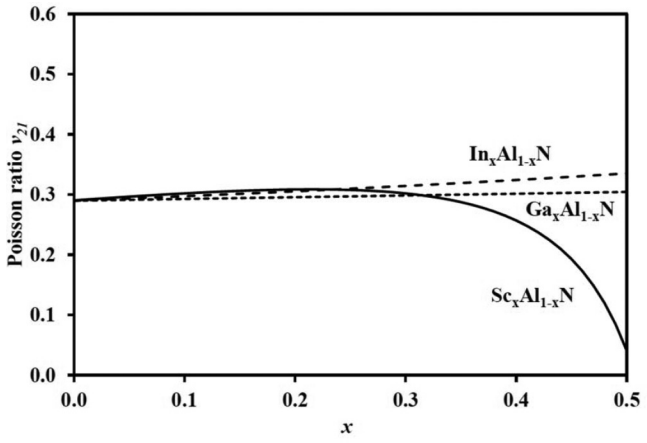

FIG. 24. Calculated Poisson ratio ν_{21} for longitudinal uniaxial extension of wurtzite $Sc_xAl_{1-x}N$ crystals in the basal plane vs metal atom concentration x (solid line). The linear interpolation between the two relevant binary nitrides for $Ga_xAl_{1-x}N$ and $In_xAl_{1-x}N$ (dashed lines) is provided for comparison.

VI. PIEZOELECTRIC POLARIZATION

The piezoelectric polarization for hexagonal materials belonging to the C_{6v} crystallographic point group is given by[57]

$$P_{PE,i} = \sum_l d_{il}\sigma_l, \quad i = 1,\ 2,\ 3, \quad l = 1,\ \ldots,\ 6, \tag{35}$$

where $P_{PE,i}$ are the components of the piezoelectric polarization and d_{il} are the coefficients of the piezoelectric moduli matrix. Using the relations given by symmetry between the piezoelectric moduli, $d_{31} = d_{32}$, $d_{33} \neq 0$, $d_{15} = d_{24}$, and all other components $d_{il} = 0$, Eq. (35) can be reduced to

$$P_{PE,1} = \frac{1}{2} d_{15}\sigma_5, \tag{36a}$$

$$P_{PE,2} = \frac{1}{2} d_{15}\sigma_4, \tag{36b}$$

$$P_{PE,3} = d_{31}(\sigma_1 + \sigma_2) + d_{33}\sigma_3. \tag{36c}$$

More often than the piezoelectric moduli, the piezoelectric coefficients e_{kl} are used to describe the piezoelectric properties of group-III-nitrides. They can be calculated by

$$e_{kl} = \sum_j d_{kj}C_{jl}, \quad \text{where } k = 1, 2, 3, \quad l = 1, \ldots, 6, \quad j = 1, \ldots, 6 \tag{37}$$

and represented by

$$e_{kl} = \begin{pmatrix} 0 & 0 & 0 & 0 & e_{15} & 0 \\ 0 & 0 & 0 & e_{15} & 0 & 0 \\ e_{31} & e_{31} & e_{33} & 0 & 0 & 0 \end{pmatrix}. \tag{38}$$

We have computed a full set of relevant piezoelectric coefficients e_{kl} (in units of C/m^2) of $Sc_xAl_{1-x}N$[10] and described them by a quadratic function, thereby constraining the function at $x = 0$ to the piezoelectric coefficients of AlN,

$$e_{15}^{\mathrm{ScAlN}}(x) = 0.308\ x - 0.313\ (1-x) - 0.528\ x\ (1-x), \tag{39a}$$

$$e_{31}^{\mathrm{ScAlN}}(x) = -1.353\ x - 0.593\ (1-x) + 0.576\ x\ (1-x), \tag{39b}$$

$$e_{33}^{\mathrm{ScAlN}}(x) = 9.125\ x + 1.471\ (1-x) - 6.625\ x\ (1-x)\ . \tag{39c}$$

The results for the symmetrized piezoelectric tensor components are presented in Figs. 25–27 and vary significantly as a function of x. While e_{15}^{ScAlN} increases by 58%, the negative value of e_{31}^{ScAlN} increases by 42%, when x is enhanced from 0 up to 0.5. Most notably, e_{33}^{ScAlN} increases nonlinear by more than 140% when comparing $Sc_{0.5}Al_{0.5}N$ to AlN $\left(e_{33}^{\mathrm{ScAlN}}(x=0.5) = 3.641\ \frac{C}{m^2} > e_{33}^{\mathrm{ScAlN}}(x=0) = 1.471\ \frac{C}{m^2}\right)$. Compared to the piezoelectric coefficients of GaAlN and InAlN, the

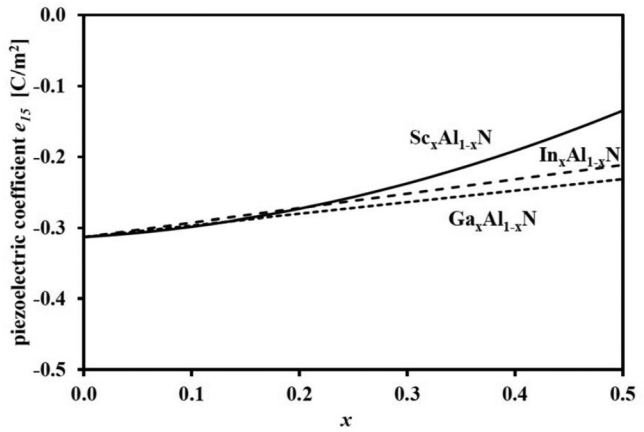

FIG. 25. Calculated piezoelectric coefficient e_{15} vs metal atom concentration x for $Sc_xAl_{1-x}N$ alloys with the wurtzite crystal structure (solid line). The values for $Ga_xAl_{1-x}N$ and $In_xAl_{1-x}N$ (dashed lines) are provided for comparison.

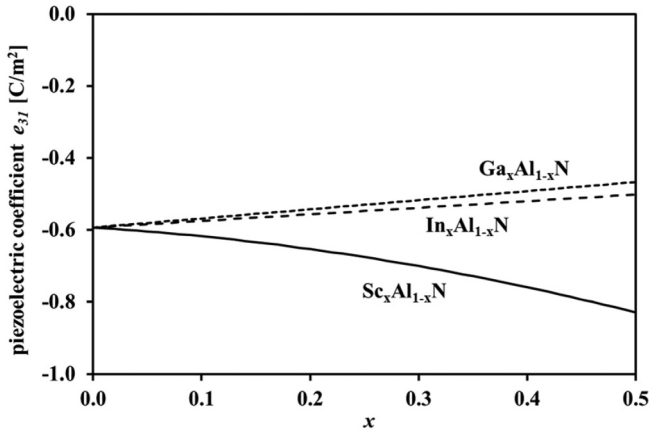

FIG. 26. Calculated piezoelectric coefficient e_{31} vs metal atom concentration x for $Sc_xAl_{1-x}N$ alloys with the wurtzite crystal structure (solid line). The linear interpolation between the two relevant binary nitrides for $Ga_xAl_{1-x}N$ and $In_xAl_{1-x}N$ (dashed lines) are shown for comparison.

increase of e_{15}^{ScAlN} is twice as large when half of the Al atoms are substituted, whereas e_{31}^{ScAlN} is significantly decreased in the same range of x, it increases for GaAlN and InAlN and whereas e_{33}^{ScAlN} is strongly enlarged, it is reduced by 27% and 22% for GaAlN and InAlN, respectively. Using the piezoelectric coefficients calculated and discussed above, we can determine also a full set of piezoelectric moduli. For hexagonal crystals, the relations between piezoelectric coefficients and moduli can be reduced to

$$\begin{aligned} e_{31} &= e_{32} = C_{11}d_{31} + C_{12}d_{32} + C_{13}d_{33} \\ &= (C_{11} + C_{12})d_{31} + C_{13}d_{33}, \end{aligned} \tag{40a}$$

$$e_{33} = 2C_{13}d_{31} + C_{33}d_{33}, \tag{40b}$$

$$e_{15} = e_{24} = C_{44}d_{15}, \text{ and for all other components} \tag{40c}$$

$$e_{kl} = 0. \tag{40d}$$

Figure 28 shows the piezoelectric moduli $d_{15}(x)$, $d_{31}(x)$, and $d_{33}(x)$ of $Sc_xAl_{1-x}N$, calculated by transforming Eqs. (40a)–(40d). While $d_{15}(x)$ is not changing much by Sc incorporation into AlN, a strong nonlinear decrease of $d_{31}(x)$ and an even stronger nonlinear increase of $d_{33}(x)$ is observed for growing Sc content. The theoretical prediction for $d_{33}(x)$ is compared to experimental results for ScAlN available in the literature[6,18,58] and to the moduli determined for GaAlN and InAlN (Fig. 29, Ref. 19). Even though the experimental data from different references are not in perfect agreement, a good accordance of the theoretical and most of the experimental results can be stated up to $x \approx 0.4$. In the case of Al substitution by Sc instead of Ga or In, a complete different behavior of $d_{33}(x)$ is observed. For an increasing concentration of Ga or In, we observe a decrease of $d_{33}(x)$, whereas a very strong and nonlinear increase is predicted and confirmed by experiment for an increasing substitution of Al by Sc atoms.

Based on a full set of piezoelectric coefficients, we are able to calculate the piezoelectric polarization of wurtzite ternary alloys, which depend on composition and strain. Because biaxial strain in epitaxial layers of group-III nitride heterostructures grown along the [0001]-axis caused by mismatch of the lattice parameter a and/or a mismatch of the thermal expansion coefficients of the layer and the substrate directed along the basal plane is of most practical relevance, we focus our further efforts on the simulation of the piezoelectric polarization for this case. In general, the piezoelectric

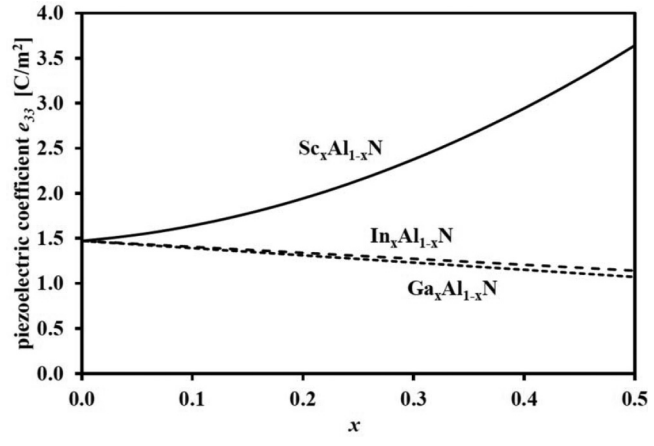

FIG. 27. Calculated piezoelectric coefficient e_{33} vs metal atom concentration x for $Sc_xAl_{1-x}N$ alloys with the wurtzite crystal structure (solid line). The linear interpolation between the two relevant binary nitrides for $Ga_xAl_{1-x}N$ and $In_xAl_{1-x}N$ (dashed lines) is provided for comparison.

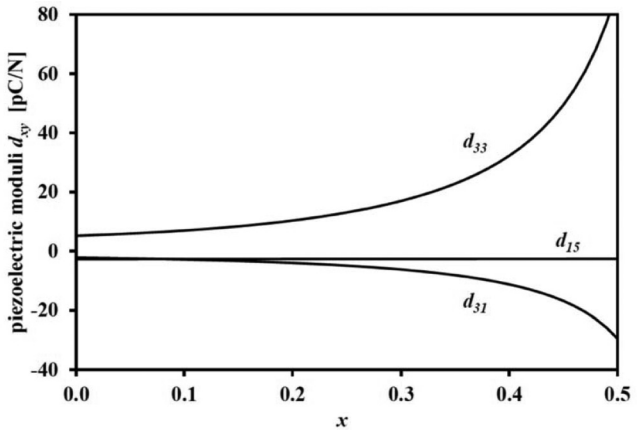

FIG. 28. Calculated piezoelectric moduli d_{15}, d_{31}, and d_{33} vs metal atom concentration x for $Sc_xAl_{1-x}N$ alloys with the wurtzite crystal structure.

polarization as a function of strain can be written as

$$P_{PE,k} = \sum_l e_{kl}\varepsilon_l, \quad \text{where } k = 1, 2, 3, \quad l = 1, \ldots, 6. \tag{41}$$

As shown before, the stiffness of the ternary compounds with wurtzite structure is isotropic in the basal plane. No force is applied on the crystals in the growth direction and they can relax freely in this direction. The resulting biaxial strain ($\varepsilon_1 = \varepsilon_2$) causes stresses $\sigma_1 = \sigma_2$, whereas σ_3 has to be zero. Using Eqs. (20) and (21), a relation between the strain along the [0001]-axis ε_3 and in the basal plane ε_1 can be derived,

$$\begin{aligned}\sigma_3 &= C_{31}\varepsilon_1 + C_{32}\varepsilon_{12} + C_{33}\varepsilon_3 = C_{13}\varepsilon_1 + C_{13}\varepsilon_2 + C_{33}\varepsilon_3 \\ &= 2C_{13}\varepsilon_1 + C_{33}\varepsilon_3 = 0,\end{aligned} \tag{42}$$

and as a consequence,

$$\varepsilon_3 = -\frac{2C_{13}}{C_{33}}\varepsilon_1. \tag{43}$$

The non-vanishing component of the piezoelectric polarization oriented along the [0001]-axis caused by biaxial strain in the basal plane is

$$P_{PE(biaxial),3} = \varepsilon_1 e_{31} + \varepsilon_2 e_{32} + \varepsilon_3 e_{33}, \tag{44}$$

$$= 2\varepsilon_1 e_{31} + \varepsilon_3 e_{33}, \tag{45}$$

$$= 2\varepsilon_1\left(e_{31} - e_{33}\frac{C_{13}}{C_{33}}\right), \text{ where } \varepsilon_1 = \frac{a - a_0}{a_0}. \tag{46}$$

In analogy, the relation between strain ε_1 and piezoelectric polarization $P_{PE,3}$ oriented along the [0001]-axis can be derived for uniaxial ($\sigma_1 = \sigma_2 = 0$, $\sigma_3 \neq 0$) and hydrostatic ($\sigma_1 = \sigma_2 = \sigma_3 \neq 0$) stresses,

$$P_{PE(uniaxial),3} = \varepsilon_1\left(e_{31} - e_{33}\frac{C_{13}}{C_{33}}\right)\left(\frac{C_{11} - C_{12}}{C_{11} - \frac{C_{13}^2}{C_{33}}}\right), \tag{47}$$

$$P_{PE(hydrostatic),3} = 2\varepsilon_1\left(2e_{31} + e_{33}\frac{C_{11} + C_{12} - 2C_{13}}{C_{33} - C_{13}}\right). \tag{48}$$

Because in all three cases, $P_{PE(stress),3}$ is proportional to the strain ε_1, Fig. 30 shows the ratio $\frac{P_{PE(stress),3}}{\varepsilon_1}$ for metal polar ScAlN in dependence on its composition. For positive strain $\varepsilon_1 > 0$, we observe over the whole range of composition investigated,

$$\frac{P^{ScAlN}_{PE(hydrostatic),3}}{\varepsilon_1} > 0, \tag{49a}$$

$$\frac{P^{ScAlN}_{PE(uniaxial),3}}{\varepsilon_1} < 0, \tag{49b}$$

$$\frac{P^{ScAlN}_{PE(biaxial),3}}{\varepsilon_1} < 0. \tag{49c}$$

This indicates that the piezoelectric polarization $P^{ScAlN}_{PE(stress),3}$ for uniaxial and biaxial strains is oriented in the same direction like the spontaneous polarization. In the case of hydrostatic stress, the piezoelectric and spontaneous polarizations are oriented antiparallel. In more detail, $\frac{P^{ScAlN}_{PE(hydrostatic),3}}{\varepsilon_1}$ shows a nonlinear strong increase

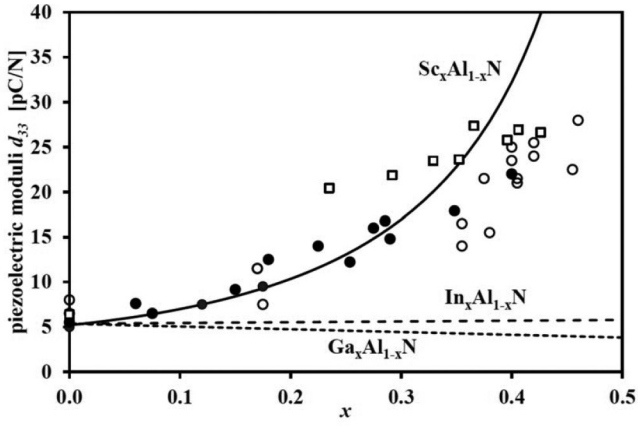

FIG. 29. Calculated (solid line) and measured (symbols: open circles,[6] black circles,[21] and open squares[58]) piezoelectric moduli d_{33} vs metal atom concentration x for $Sc_xAl_{1-x}N$ alloys with the wurtzite crystal structure. The values for $Ga_xAl_{1-x}N$ and $In_xAl_{1-x}N$ (dashed lines[19]) are shown for comparison.

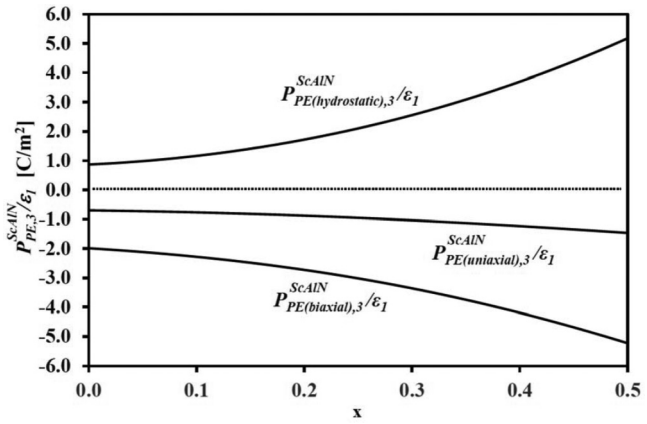

FIG. 30. Calculated ratio of piezoelectric polarization and strain ε_1 caused by uniaxial (along the [0001]-axis), biaxial (along the basal plane), and hydrostatic stresses vs metal atom concentration x for $Sc_xAl_{1-x}N$ alloys with the wurtzite crystal structure.

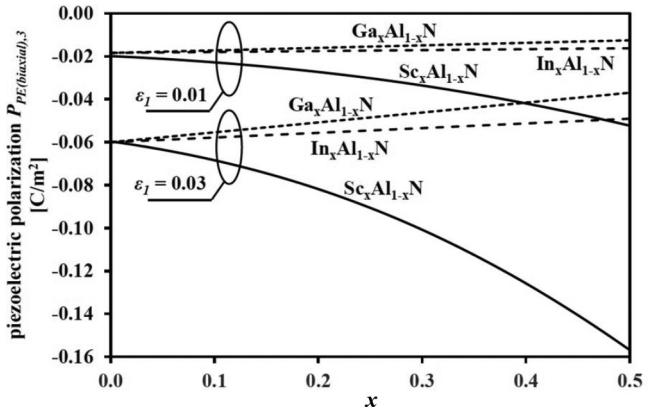

FIG. 31. Predicted piezoelectric polarization $P^{MeAlN}_{PE(biaxial),3}$ caused by biaxial strain $\varepsilon_1 = 0.01$ or $\varepsilon_1 = 0.03$ vs metal atom concentration x for metal polar $Sc_xAl_{1-x}N$ alloys with the wurtzite crystal structure (solid line). The values for $Ga_xAl_{1-x}N$ and $In_xAl_{1-x}N$ (dashed lines) are shown for comparison.

from 0.87 to 5.18 C/m^2 ($\approx$500%), if the Sc concentration is changed from $x = 0$–0.5. The value of the piezoelectric polarization caused by the biaxial strain is the highest compared to the values at the same strain ε_1 caused by hydrostatic or uniaxial stress. The value of $\frac{P^{ScAlN}_{PE(biaxial),3}}{\varepsilon_1}$ is increased nonlinear by about 160%, if half of the Al atoms are substituted by Sc. The value of $\frac{P^{ScAlN}_{PE(uniaxial),3}}{\varepsilon_1}$ shows an increase by 110% in the same range of composition. We will compare $P^{ScAlN}_{PE(biaxial),3}(x)$ with the corresponding values of GaAlN and InAlN crystals to deepen our understanding of piezoelectric polarization in wurtzitic ScAlN. In order to calculate the piezoelectric polarization of GaAlN and InAlN taking nonlinear effects into account, we follow the procedure suggested by Bernardini *et al.*[34–36] For this approach, the piezoelectric polarizations of the binary compounds are calculated first, which can be described by the relations (in C/m^2),

$$\begin{aligned} P^{AlN}_{PE(biaxial),3} &= -1.761\varepsilon_1 + 6.11\varepsilon_1^2, \text{ for } \varepsilon_1 < 0, \\ P^{AlN}_{PE(biaxial),3} &= -1.761\varepsilon_1 - 8.00\varepsilon_1^2, \text{ for } \varepsilon_1 > 0, \\ P^{GaN}_{PE(biaxial),3} &= -0.775\varepsilon_1 + 10.37\varepsilon_1^2, \\ P^{InN}_{PE(biaxial),3} &= -1.477\varepsilon_1 + 6.837\varepsilon_1^2. \end{aligned} \quad (50)$$

The piezoelectric polarization of $Me_xAl_{1-x}N$ alloys at any strain is then determined by

$$P^{MeAlN}_{PE(biaxial),3}(x) = xP^{MeN}_{PE(biaxial),3}(\varepsilon_1) + (1-x)P^{AlN}_{PE(biaxial),3}(\varepsilon_1), \quad (51)$$

where $P^{MeN}_{PE(biaxial),3}(\varepsilon_1)$ *and* $P^{AlN}_{PE(biaxial),3}(\varepsilon_1)$ are the strain dependent bulk piezoelectric polarizations of the relevant binary compounds (50). Figure 31 visualizes the piezoelectric polarizations oriented along the [0001]-axis of metal polar ternary alloys caused by biaxial strains in the basal plane corresponding to $\varepsilon_1 = 0.01$ and $\varepsilon_1 = 0.03$, respectively. We have chosen these two strain values because a biaxial tensile strain of $\varepsilon_1 = 0.01$ occurs in $Sc_{0.13}Al_{0.87}N$, $In_{0.12}Al_{0.88}N$, and $Ga_{0.64}Al_{0.36}N$ layers pseudomorphically grown on the c-plane of relaxed GaN substrates. If thin layers of AlN are epitaxially grown on GaN substrates, a biaxial strain of about 0.03 is required to match the lattice parameter a(AlN) = a_0(GaN). These heterostructures are relevant for processing energy efficient power electronic devices as discussed in Refs. 59–62. Coming back to the piezoelectric polarization caused by biaxial strain: if the number of Ga and In atoms substituting Al atoms of AlN is increased, the value of piezoelectric polarization is decreasing. This effect is more

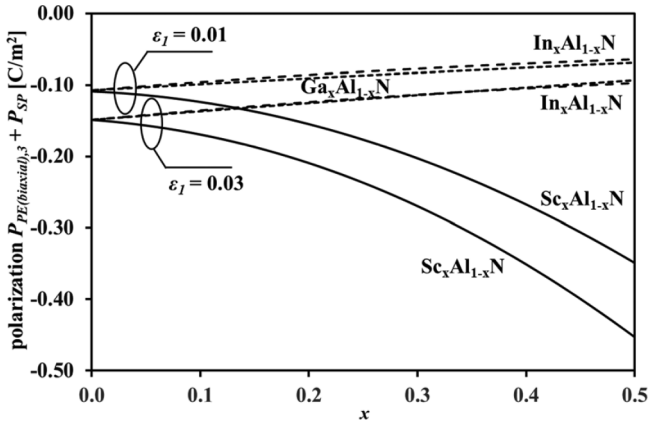

FIG. 32. Predicted total polarization $P^{MeAlN}_{PE(biaxial),3} + P^{MeAlN}_{SP}$ vs metal atom concentration x for metal polar $Sc_xAl_{1-x}N$ alloys with the wurtzite crystal structure (solid line). The piezoelectric polarization is caused by biaxial strains: $\varepsilon_1 = 0.01$ or $\varepsilon_1 = 0.03$. The corresponding values for $Ga_xAl_{1-x}N$ and $In_xAl_{1-x}N$ (dashed lines) are provided for comparison.

pronounced for the substitution by Ga in comparison to In. In contrast to this observation, the incorporation of Sc into AlN is causing a strong increase in the value of piezoelectric polarization at a given strain. A similar observation is made for the total polarization $P_{PE(biaxial),3}(x) + P_{SP}(x)$ calculated for $\varepsilon_1 = 0.01$ and $\varepsilon_1 = 0.03$, respectively (Fig. 32). Whereas the values of the total polarization of GaAlN and InAlN in comparison to AlN are decreased between 35% and 40% for both strains chosen, the polarization value of ScAlN is increased by about 220% for $\varepsilon_1 = 0.01$ and 200% for $\varepsilon_1 = 0.03$, respectively, when x is enlarged to 0.5. It should be pointed out that over the whole range of composition, the value (and the nonlinearity) of the total polarization is dominated by the value of spontaneous polarization of $Sc_xAl_{1-x}N$, which contributes 81%–84% for $\varepsilon_1 = 0.01$ and 60%–65% for $\varepsilon_1 = 0.03$ to the total polarization value, respectively. For metal polar ScAlN films with a biaxial strain of $\varepsilon_1 = 0.03$, deposited by molecular beam epitaxy,[63,64] metal-organic chemical vapor deposition,[65] or reactive ion sputtering,[6,18,58] the total polarization is calculated to reach a value of 0.267 $C\,m^{-2}$, which is the highest polarization within the group-III-nitrides predicted up to date.

VII. SUMMARY

In summary, we have determined by simulations and experiments that wurtzite ScAlN shows outstanding structural, mechanical, and polarization related properties compared to other group-III nitride ternary alloys like GaAlN and InAlN. As a consequence of an increasing random Sc incorporation on metal lattice sides, the structural geometry of wurtzite $Sc_xAl_{1-x}N$ deviates more and more from an ideal hexagonal crystal lattice in a way that it resembles a crystal deformed by virtual biaxial tensile strain oriented in basal plane. The deviation away from ideal tetrahedral bonding is accompanied by an approximately linear increase of average bond lengths and lattice parameter $a(x)$ as well as a nonlinear change of bond angles and lattice parameter $c(x)$. The elastic quantities of $Sc_xAl_{1-x}N$ such as the average bulk modulus B, shear modulus G, and the Young modulus E indicate a softening and an increasing anisotropy of stiffness in the $(0001)/(2\bar{1}\bar{1}0)$-plane. The average bond ionicity increases with increasing Sc content, which is expected because of the higher ionicity of Sc–N bonds in ScN compared to Ga–N and Al–N bonds in GaN and AlN. DFT computations indicate a higher electron density surrounding the N atoms adjacent to a Sc atom than the N atoms adjacent only to Ga or Al atoms. The increasing ionicity in combination with the enhancement of structural deformation is causing a strong enlargement of spontaneous polarization values. The spontaneous polarization of wurtzite AlN is increased in a nonlinear manner, reaching a theoretical predicted value of about 0.3 C/m^2 for $x = 0.5$. In addition, we find an outstanding increase of the piezoelectric coefficient e_{33} and moduli d_{33} reaching 2.94 C/m^2 and 32.25 pC/N for $x = 0.4$, respectively. The softening of AlN and the enlargement of $|e_{33}(x)|$ and $|e_{31}(x)|$ caused by an increased incorporation of Sc causes a nonlinear strong growing value of the piezoelectric polarization at constant (hydrostatic and) biaxial strain. This is remarkable because the substitution of Al atoms of AlN crystals by Ga and In is causing a reduction of the piezoelectric polarization value at constant biaxial strain. For biaxial strains up to 0.03, which are experimentally observed as maximum value in GaN-based heterostructures relevant for applications, the spontaneous polarization of $Sc_xAl_{1-x}N$ crystals is dominating the total polarization oriented along the [0001]-axis and its nonlinear enlargement by increasing x. For biaxial strained $Sc_{0.4}Al_{0.6}N$-layers, we predict total polarizations values of up to 0.45 C/m^2.

ACKNOWLEDGMENTS

This work was partially supported by the German Science Foundation (DFG) Project No. AM 105/40-1. In addition, the work was partially supported by the Gips-Schüle-Stiftung and the Carl-Zeiss-Stiftung (project "SCHARF"). The authors would like to thank T. Fuchs for assistance with the SIMS measurements, M. Baeumler for optical analysis, N. Kurz for characterization of piezoelectric coefficients, as well as the members of the departments "Epitaxy" and "Technology" at Fraunhofer IAF for their assistance in the deposition of ScAlN-based films and the processing of devices. Last but not least, the authors would like to thank Evatec AG, the thin film powerhouse, for providing samples and equipment.

DATA AVAILABILITY

The data that support the findings of this study are available from the corresponding author upon reasonable request.

REFERENCES

[1]W. Tian, Z. Ling, W. Yu, and J. Shi, "A review of MEMS scale piezoelectric energy harvester," Appl. Sci. **8**, 645 (2018).
[2]A. Mohanty, S. Parida, R. K. Behera, and T. Roy, "Vibration energy harvesting: A review," J. Adv. Dielectr. **9**, 1930001 (2019).
[3]Q. Chen and Q.-M. Wang, "The effective electromechanical coupling coefficient of piezoelectric thin-film resonators," Appl. Phys. Lett. **86**, 022904 (2005).
[4]N. Setter, D. Damjanovic, L. Eng, G. Fox, S. Gevorgian, S. Hong, A. Kingon, H. Kohlstedt, N. Y. Park, G. B. Stephenson, I. Stolitchnov, A. K. Taganstev, D. V. Taylor, T. Yamada, and S. Streiffer, "Ferroelectric thin films: Review of materials, properties, and applications," J. Appl. Phys. **100**, 051606 (2006).
[5]T. Kim, J. Kim, R. Dalmau, R. Schlesser, E. Preble, and X. Jiang, "High-temperature electromechanical characterization of AlN single crystals," IEEE Trans. Ultrason. Ferroelectr. Freq. Control **62**(10), 1880 (2015).
[6]M. Akiyama, T. Kamohara, K. Kano, A. Teshigahara, Y. Takeuchi, and N. Kawahara, "Enhancement of piezoelectric response in scandium aluminum nitride alloy thin films prepared by dual reactive cosputtering," Adv. Mater. **21**, 593 (2009).
[7]W. Wang, P. M. Mayrhofer, X. He, M. Gillinger, Z. Ye, X. Wang, A. Bittner, U. Schmid, and J. K. Luo, "High performance AlScN thin film based surface acoustic wave devices with large electromechanical coupling coefficient," Appl. Phys. Lett. **105**, 133502 (2014).
[8]S. Takayanagi, T. Yanagitani, and M. Matsukawa, "c-Axis tilted or c-axis parallel ScAlN films/substrate SAW devices with high electromechanical coupling," Proc. Symp. Ultrason. Electron. **34**, 143 (2013).
[9]T. Yanagitani and M. Suzuki, "Electromechanical coupling and gigahertz elastic properties of ScAlN films near phase boundary," Appl. Phys. Lett. **105**, 122907 (2014).
[10]D. F. Urban, O. Ambacher, and C. Elsässer, "First-principles calculation of electroacoustic properties of wurtzite (Al, Sc) N," Phys. Rev. B **103**, 115204 (2021).
[11]See https://www.quantum-espresso.org/ for an integrated suite of Open-Source computer codes for electronic-structure calculations and materials modeling at the nanoscale.

[12]P. Giannozzi *et al.*, "QUANTUM ESPRESSO: A modular and open-source software project for quantum simulations of materials," J. Phys.Condens. Matter **21**, 395502 (2009).
[13]G. Prandini, A. Marrazzo, I. E. Castelli, N. Mounet, and N. Marzari, "A standard solid state pseudopotentials library optimized for accuracy and efficiency (version 1.0)," Materials Cloud Archive (2018).
[14]K. Lejaeghere *et al.*, "Reproducibility in density functional theory calculations of solids," Science **351**, 1415 (2016).
[15]C. Höglund, J. Birch, B. Alling, J. Bareno, Z. Czigany, P. O. A. Persson, G. Wingqvist, A. Zukauskaite, and L. Hultman, "Wurtzite structure $Sc_{1-x}Al_xN$ solid solution films grown by reactive magnetron sputter epitaxy: Structural characterization and first-principles calculations," J. Appl. Phys. **107**, 123515 (2010).
[16]F. Tasnadi, B. Alling, C. Höglund, G. Wingqvist, J. Birch, L. Hultman, and I. A. Abrikososv, "Origin of the anomalous piezoelectric response in wurtzite $Sc_xAl_{1-x}N$ alloys," Phys. Rev. Lett. **104**, 137601 (2010).
[17]S. Zhang, W. Y. Fu, D. Holec, C. J. Humphreys, and M. A. Moram, "Elastic constants and critical thicknesses of ScGaN and ScAlN," J. Appl. Phys. **114**, 243516 (2013).
[18]H. Momida, A. Teshigahara, and T. Oguchi, "Strong enhancement of piezoelectric constants in $Sc_xAl_{1-x}N$: First-principles calculations," AIP Adv. **6**, 065006 (2006).
[19]O. Ambacher, J. Majewski, C. Miskys, A. Link, M. Hermann, M. Eickhoff, M. Stutzmann, F. Bernardini, V. Fiorentini, V. Tilak, B. Schaff, and L. F. Eastman, "Pyroelectric properties of Al(In)GaN/GaN hetero-and quantum well structures," J. Phys. Condens. Matter **14**, 3399 (2002).
[20]V. Darakchieva, M. Y. Xie, F. Tasnadi, I. A. Abrikosov, L. Hultman, B. Monemar, J. Kamimura, and K. Kishino, "Lattice parameters, deviations from Vegard's rule, and E_2 phonons in InAlN," Appl. Phys. Lett. **93**, 261908 (2008).
[21]Y. Lu, M. Reusch, N. Kurz, A. Ding, T. Christoph, M. Prescher, L. Kirste, O. Ambacher, and A. Zukauskaite, "Elastic modulus and coefficient of thermal expansion of piezoelectric $Al_{1-x}Sc_xN$ (up to $x = 0.41$) thin films," Appl. Phys. Lett. Mater. **6**, 076105 (2018).
[22]N. Herres, L. Kirste, H. Obloh, K. Köhler, J. Wagner, and P. Koidl, "X-ray determination of the composition of partially strained group-III nitride layers using the extended bond method," Mater. Sci. Eng. B **91–92**, 425 (2002).
[23]R. Deng, S. R. Evans, and D. Gall, "Bandgap in $Al_{1-x}Sc_xN$," Appl. Phys. Lett. **102**, 112103 (2013).
[24]N. Kurz, "Untersuchung der elektroakustischen und pyroelektrischen Eigenschaften von Aluminium-Scandium-Nitrid für mikroakustische Hochfrequenzfilter," Dissertation (Albert-Ludwigs-Universität Freiburg, 2019).
[25]L. Vegard, "Die Konstitution der Mischkristalle und die Raumfüllung der Atome," Z. Phys. **5**, 17 (1921).
[26]S. Barth, H. Bartzsch, D. Gloess, P. Frach, T. Modes, O. Zywitzki, G. Suchaneck, and G. Gerlach, "Influence of process parameters on properties of piezoelectric AlN and AlScN thin films for sensor and energy harvesting applications," Proc. SPIE **9517**, 951704 (2015).
[27]R. Gross and A. Marx, *Festkörperphysik* (Oldenbourg Wissenschaftsverlag, 2012).
[28]C. Kittel, *Einführung in die Festkörperphysik* (Oldenbourg Wissenschaftsverlag, 2006).
[29]W. Borchardt-Ott and H. Sowa, *Kristallographie Eine Einführung für Naturwissenschaftler* (Springer Spektrum, 2013).
[30]G. Wingqvist, F. Tasnádi, A. Zukauskaite, J. Birch, H. Arwin, and L. Hultman, "Increased electromechanical coupling in w−$Sc_xAl_{1-x}N$," Appl. Phys. Lett. **97**, 112902 (2010).
[31]R. Matloub, M. Hadad, A. Mazzalai, N. Chidambaram, G. Moulard, C. S. Sandu, T. Metzger, and P. Muralt, "Piezoelectric $Al_{1-x}Sc_xN$ thin films: A semiconductor compatible solution for mechanical energy harvesting and sensors," Appl. Phys. Lett. **102**, 152903 (2013).
[32]T. Mattila and A. Zunger, "Predicted bond length variation in wurtzite and zinc-blende InGaN and AlGaN alloys," J. Appl. Phys. **85**, 160 (1999).
[33]A. Zoroddu, F. Bernardini, P. Ruggerone, and V. Fiorentini, "First-principles prediction of structure, energetics, formation enthalpy, elastic constants, polarization, and piezoelectric constants of AlN, GaN, and InN: Comparison of local and gradient-corrected density-functional theory," Phys. Rev. B **64**, 45208 (2001).
[34]F. Bernardini, V. Fiorentini, and D. Vanderbilt, "Spontaneous polarization and piezoelectric constants of III-V nitrides," Phys. Rev. B **56**, R10024 (1997).
[35]F. Bernardini and V. Fiorentini, "Nonlinear macroscopic polarization in III-V nitride alloys," Phys. Rev. B **64**, 85207 (2001).
[36]F. Bernardini and V. Fiorentini, "Nonlinear behavior of spontaneous and piezoelectric polarization in III–V nitride alloys," Phys. Status Solidi A **190**, 65 (2002).
[37]M. A. Caro, S. Zhang, T. Riekkinen, M. Ylilammi, M. A. Moram, O. Lopez-Acevedo, J. Molarius, and T. Laurila, "Piezoelectric coefficients and spontaneous polarization of ScAlN," J. Phys. Condens. Matter **27**, 245901 (2015).
[38]D. Vanderbilt and R. D. King-Smith, "Electric polarization as a bulk quantity and its relation to surface charge," Phys. Rev. B **47**, 1651 (1993).
[39]R. Resta, "Macroscopic polarization in crystalline dielectrics: The geometric phase approach," Rev. Mod. Phys. **66**, 899 (1994).
[40]C. E. Dreyer, A. Janotti, C. G. Van de Walle, and D. Vanderbilt, "Correct implementation of polarization constants in wurtzite materials and impact on III-nitrides," Phys. Rev. X **6**, 021038 (2016).
[41]A. F. Wright, "Elastic properties of zinc-blende and wurtzite AlN, GaN, and InN," J. Appl. Phys. **82**, 2833 (1997).
[42]P. Hohenberg and W. Kohn, "Density functional theory," Phys. Rev. B **136**, 864 (1964).
[43]J. P. Perdew, K. Burke, and M. Ernzerhof, "Perdew, Burke, and Ernzerhof reply," Phys. Rev. Lett. **77**, 3865 (1996).
[44]S. P. Łepkowski, J. A. Majewski, and G. Jurczak, "Nonlinear elasticity in III-N compounds: *Ab initio* calculations," Phys. Rev. B **72**, 245201 (2005).
[45]A. Polian, M. Grimsditch, and I. Grzegory, "Elastic constants of gallium nitride," J. Appl. Phys. **79**, 3343 (1996).
[46]C. Deger, E. Born, H. Angerer, O. Ambacher, M. Stutzmann, J. Hornstein, E. Riha, and G. Fischerauer, "Sound velocity of $Al_xGa_{1-x}N$ thin films obtained by surface acoustic-wave measurements," Appl. Phys. Lett. **72**, 2400 (1998).
[47]K. Tsubouchi and N. Mikoshiba, "Zero-temperature-coefficient SAW devices on AlN epitaxial films," IEEE Trans. Sonics Ultrason. **32**, 634 (1985).
[48]M. Moreira, J. Bjurström, I. Katardjev, and V. Yantchev, "Aluminum scandium nitride thin-film bulk acoustic resonators for wide band applications," Vacuum **86**, 23 (2011).
[49]M. J. Mehl, B. K. Klein, and D. A. Papaconstanttopoulos, "Intermetallic compound principle and practice," in *Principles*, edited by J. H. Westbrook and R. L. Fleischer (John Wiley and Sons, 1995), Vol. I.
[50]W. Voigt, *Lehrbuch der Kristallphysik* (Taubner, Leipzig, 1928).
[51]E. Schreiber, O. L. Anderson, and N. Soga, *Elastic Constants and Their Measurements* (McGraw-Hill, New York, 1923), pp. 23–25.
[52]O. Zywitzki, T. Modes, S. Barth, H. Bartzsch, and P. Frach, "Effect of scandium content on structure and piezoelectric properties of AlScN films deposited by reactive pulse magnetron sputtering," Surf. Coat. Technol. **309**, 417 (2017).
[53]J. Tan, Y. Li, and G. Ji, "Elastic constants and bulk modulus of semiconductors: Performance of plane-wave pseudopotential and local-density-approximation density functional theory," Comput. Mater. Sci. **58**, 243 (2012).
[54]J. C. Phillips, *Bonds and Bands in Semiconductors* (Academic Press, 1973).
[55]B. Jogai, "Three-dimensional strain field calculations in multiple InN/AlN wurtzite quantum dots," J. Appl. Phys. **90**, 699 (2001).
[56]A. Ballato, "Piezoelectricity: Old effect, new thrusts," IEEE Trans. Ultrason. Ferroelectr. Freq. Control **43**, 56 (1995).
[57]J. F. Nye, *Physical Properties of Crystals, Their Representation by Tensors and Matrices* (Clarendon, Oxford, 1985).
[58]P. Frach, S. Barth, H. Bartzsch, and D. Gloess, "Energy harvesting based on piezoelectric AlN and AlScN thin films deposited by high rate sputtering," Proc. SPIE **10194**, 101942Z (2017).

[59]M. Basler, R. Reiner, S. Moench, P. Waltereit, R. Quay, I. Kallfass, and O. Ambacher, "Large-area lateral AlGaN/GaN-on-Si field-effect rectifier with low turn-on voltage," IEEE Electron Device Lett. **41**, 993 (2020).
[60]F. Medjdoub, M. Zegaoui, D. Ducatteau, N. Rolland, and P. A. Rolland, "High-performance low-leakage-current AlN/GaNHEMTs grown on silicon substrate," IEEE Electron Device Lett. **32**, 874 (2011).
[61]J. Ligl, S. Leone, C. Manz, L. Kirste, P. Doering, T. Fuchs, and M. Prescher, "Metalorganic chemical vapor phase deposition of AlScN/GaN heterostructures," J. Appl. Phys. **127**, 195704 (2020).
[62]T. E. Kazior, E. M. Chumbes, B. Schultz, J. Logan, D. J. Meyer, and M. T. Hardy, in *IEEE MTT-S International Microwave Symposium* (IEEE, 2019).
[63]M. T. Hardy, B. P. Downey, N. Nepal, D. F. Storm, D. S. Katzer, and D. J. Meyer, "Epitaxial ScAlN grown by molecular beam epitaxy on GaN and SiC substrates," Appl. Phys. Lett. **110**, 162104 (2017).
[64]K. Frei, R. Trejo-Hernández, S. Schütt, L. Kirste, M. Prescher, R. Aidam, S. Müller, P. Waltereit, O. Ambacher, and M. Fiederle, "Investigation of growth parameters for ScAlN-barrier HEMT structures by plasma-assisted MBE," Jpn. J. Appl. Phys. **58**, SC1045 (2019).
[65]S. Leone, J. Ligl, C. Manz, L. Kirste, T. Fuchs, H. Menner, M. Prescher, J. Wiegert, A. Žukauskaitė, R. Quay, and O. Ambacher, "Metal-organic chemical vapor deposition of aluminum scandium nitride," Phys. Status Solidi RRL **14**, 1900535 (2020).